Experimental Astronomy (2023) 56:371–402
https://doi.org/10.1007/s10686-023-09918-4

RESEARCH

Relativistic particle measurement in jupiter's magnetosphere with Pix.PAN

Johannes Hulsman[1] · Xin Wu[1] · Philipp Azzarello[1] · Benedikt Bergmann[2] · Michael Campbell[3] · George Clark[4] · Franck Cadoux[1] · Tomoya Ilzawa[1] · Peter Kollmann[4] · Xavi Llopart[3] · Quentin Nénon[5] · Mercedes Paniccia[1] · Elias Roussos[6] · Petr Smolyanskiy[2] · Daniil Sukhonos[1] · Pierre Alexandre Thonet[7]

Received: 27 March 2023 / Accepted: 31 October 2023 / Published online: 18 November 2023

Abstract

Pix.PAN is a compact cylindrical magnetic spectrometer, intended to provide excellent high energy particle measurements under high rate and hostile operating conditions in space. Its principal design is composed of two Halbach-array magnetic sectors and six Timepix4-based tracking layers; the latest hybrid silicon pixel detector readout ASIC designed. Due to Pix.PAN's compact and relatively simple design, it has the potential to be used for space missions exploring with measurements of unprecedented precision, high energy particles in radiation belts and the heliophere (solar energetic particles, anomalous and galactic cosmic rays). In this white paper, we discuss the design and expected performance of Pix.PAN for COMPASS (**C**omprehensive **O**bservations of **M**agnetospheric **P**article **A**cceleration, **S**ources, and **S**inks), a mission concept submitted to NASA's Call "B.16 Heliophysics Mission Concept Studies (HMCS)" in 2021 that targets the extreme high energy particle environment of Jupiter's inner radiation belts. We also discuss PixPAN's operational conditions and interface requirements. The conceptual design shows that is possible to achieve an energy resolution of <12% for electrons in the range of 10 MeV-1 GeV and <35% for protons between ∼200 MeV to a few GeV. Due to the timestamp precision of Timepix4, a time resolution (on an instrument level) of about 100 ps can be achieved for time-of-flight measurements. In the most intense radiation environments of the COMPASS mission, Pix.PAN is expected to have a maximum hit rate of $44\frac{\text{MHz}}{\text{cm}^2}$ which is below the design limit of $360\frac{\text{MHz}}{\text{cm}^2}$ of Timepix4. Finally, a sensor design is proposed which allows the instrument to operate with a power budget of 20W without the loss of scientific performance.

✉ Johannes Hulsman
johannes.hulsman@unige.ch

✉ Xin Wu
xin.wu@unige.ch

Extended author information available on the last page of the article

Keywords Pix.PAN · Timepix4 · Radiation · Radiation belt · Cosmic rays

1 Motivation

Before the launch of the satellite Explorer 1 on January 1st 1958, scientists expected that charged particles could be trapped and form radiation belts. However, they expected this to only occur during magnetic storms and therefore only exist temporarily. The Explorer 1 was launched into an elliptical orbit with an altitude between 358 and 2550 km, carrying a Geiger counter developed by a group at the University of Iowa, led by James van Allen. The device was designed to measure high energy ions (above 30 MeV) and electrons (above 3 MeV). Unexpectedly, it discovered a high count rate starting at about 1000 km. Early findings were puzzling, but later understood to be a characteristic feature when exposed to too high radiation environments. This was later confirmed with the launch of the Explorer 3 satellite. Van Allen quickly understood that these high radiation areas are due to trapped charged particles in Earth's magnetic field, leading to the birth of the Van Allen Belts. [1, 2].

It stands to reason that any other planet which is sufficiently magnetized would therefore also host radiation belts. This was confirmed for Jupiter, Saturn, Uranus and Neptune [3, 4]. For Jupiter, its existence was first inferred through radio emissions in the 1950s and later observed by Pioneer 10 in 1973 [5]. The radiation belts at Saturn were first observed by Pioneer 11 in 1979 [6]. Voyager 2, the only probe so far, was only able to nominally prove the existence of radiation belts near Neptune and Uranus. Naturally, high energy particles can also be found in other regions besides these radiation belts. They can be found throughout the planetary magnetosphere, in the interstellar and intergalactic medium, in brown dwarfs or astrospheres of stars [7]. For the study of galactic cosmic rays (GCRs), simply measuring the particles in space is insufficient to understand its origins and acceleration sites. Fortunately, radiation belts allow for in-situ measurements to study the high energy physics processes (in time scales of space missions). Combined with remote observations, the results allow to further constrain models characterizing large scale astrophysical systems.

Owing to the growing interest in the research community and launch of many missions in the past 65 years, much has been discovered about the Earth's radiation belts in terms of structure, origin and dynamical evolution. For example, it is now know that there are two stable radiation belts around Earth[1]. Two dominant sources of the high energy proton population in the inner belt (energies exceeding 100 MeV) have now been identified: i) Cosmic Ray Albedo Neutron Decays (CRANDs), a process where cosmic rays (comprised of 90% protons at energies well above >10 MeV) strike nuclei in the atmosphere, producing a shower of secondary particles, some of which are free neutrons that escape decay into protons [8] (see Fig. 1), ii) solar energetic protons from coronal mass ejections and flares [9]. The outer radiation belt consists primarily of electrons with energies ranging from 100 keV to 10 MeV and is more susceptible to the solar activity. These populations are produced through a combination of local energy

[1] A third radiation belt was discovered by the Van Allen Probes as a product of coronal mass ejections. These are unstable and generally merge with the outer belt after a few weeks.

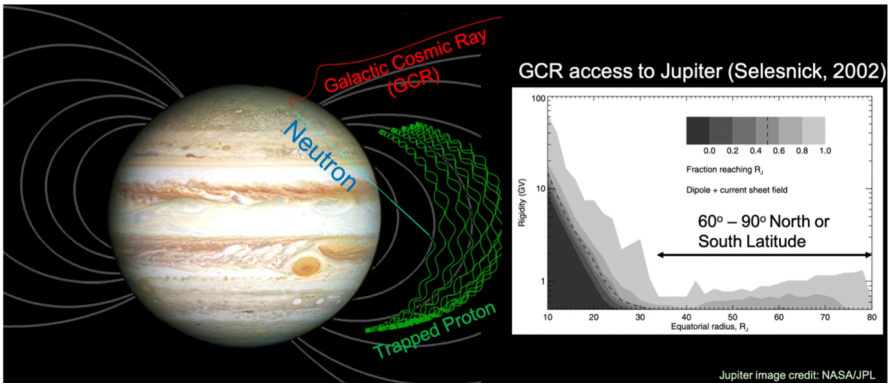

Fig. 1 Artistic illustration of the CRAND process at Jupiter with the GCR cutoff rigidities at its magnetosphere [14, 15]

transfer and inward radial diffusion [10, 11]. The Van Allen Probes which launched on August 30th 2012 and operated for 7 years yielded further significant strides in the field. Among the many findings [12], they showed that a temporary third electron storage ring (for energies $\geq$2 MeV) appears during intense solar activities. They also found that, unlike the outer belt, no electrons with energies above 1 MeV could be found in the inner belt (at low altitudes). In combination with a balloon experiment (BARREL [13]), they found that particle's acceleration and subsequent breaking out of the belt (and traversing to Earth) was linked to their electric charge and not their mass. Their combined results have therefore greatly improved the predictability of relativistic ion and electron populations and dynamics with respect to the interplay with the solar activity.

Jupiter is of particular interest as its magnetic moment is 20,000 times stronger than that of the Earth; it is the most intense in the solar system. There, particles have been observed with energies in excess of 70 MeV and 1 GeV for electrons and protons respectively [16, 17]. For protons, these energies can be as high as 100 GeV, almost 50 times higher than what can be trapped on Earth. The contribution of electrons in the radiation belt can be recognized through its synchrotron emission with the Karl G. Jansky Very Large Array (VLA) [18], Low-Frequency Array (LOFAR) [19] and/or Giant Metrewave Radio Telescope (GMRT) [20]. Jupiter's inner magnetosphere is influenced by a number of moons and satellites embedded in it. Io's extreme volcanic activity, Europa's sub-surface ocean, and the irregular inner satellites, such as Amalthea, shape the radiation belts via an intriguing combination of source and loss processes. Jupiter's fast rotation and material from Io's volcanoes that fills the system, aid the magnetic field to push against the solar wind even further, leading to a magnetosphere of enormous dimensions [21] within the volume of which, numerous combinations of source, loss and acceleration processes may be operating that cannot be realized at smaller systems like Earth, or even Saturn.

Despite being studied for decades, the hazardous environment generated by the extreme fluxes of penetrating particle radiation near the planet, has prevented us so far from observing the most interesting region of Jupiter's radiation belts in a com-

prehensive way (with spacecrafts). Therefore, many fundamental questions remain unresolved, especially with regards to particle source and acceleration to very high energies. To date, few missions have approached Jupiter closer than its moon Io (which is at 5.9 R_j). Pioneer 10/11 performed flybys and carried energetic particle detectors; although these suffered from both saturation and degradation. Voyager 1 experienced radiation damage [22]. Galileo performed many orbits through the equatorial belts, albeit for >5 R_j. Three orbits were within Io's orbital limit but several of its energetic particle detectors suffered problems with saturation and radiation damage. Juno [23] regularly passes through the inner belts (from high latitudes) but is not instrumented for the highest energy particles that are of interest here. In short, past and current missions were either insufficiently instrumented or did not approach Jupiter's radiation belts close enough.

Cassini, a mission which orbited Saturn for 13 years, only performed a flyby to obtain a gravity assist to reach Saturn. At the end of Cassini's mission, it approached an uncharted region between the planet (Saturn) itself and the innermost D-ring. This spawned new discoveries [24]. Among them was the discovery of a new innermost radiation belt [25] whose population could primarily originate through the CRAND process. This does not imply that this is also to be expected at Jupiter. It merely emphasizes that the exploration of Jupiter's radiation belt (with proper instrumentation) could lead to many new discoveries.

In 2019, a White Paper was submitted to Experimental Astronomy, titled "The in-situ exploration of Jupiter's radiation belts", in response to the ESA's Voyage 2050 Call [7]. The paper argues that Jupiter's radiation belts and the vast magnetosphere that encloses them constitute an unprecedented natural laboratory suitable for both interdisciplinary and novel scientific investigations. From the perspective of ultra-relativistic particles, an in-situ measurement will allow for ground-breaking advances in all five outstanding science investigations as identified in the Voyage 2050 White Paper. These are:

1. Adiabatic electron heating vs local electron radiation belt sources and losses;
2. Cosmic Ray Albedo Neutron Decay as universal proton radiation belt source;
3. The enigmatic origin of the heavy and light ion radiation belts;
4. High latitude charged particle acceleration as a universal radiation belt source;
5. The space weather of Jupiter's radiation belts;

A novel mission concept to probe these fundamental science investigations, in addition to other mysteries, is being developed by NASA, but has significant international contributions. The mission concept is called Comprehensive Observations of Magnetospheric Particle Acceleration, Sources, and Sinks (COMPASS) and was funded by NASA in preparation for the 2024-2033 National Academies of Science Decadal Survey in Solar and Space Physics ([15]). COMPASS is designed to explore the uncharted and hazardous regions of Jupiter's radiation belts with highly capable instrumentation. One important goal of COMPASS is to measure the relativistic electron and ion populations, ranging from eV to GeV, that form Jupiter's intense radiation belts (see Fig. 2 for a more detailed overview). The final report was submitted to NASA on 21/Oct/2022. At the time of writing, the report is not yet publicly available. However, a summary in the form of a white paper is available through [26]. Pix.PAN is

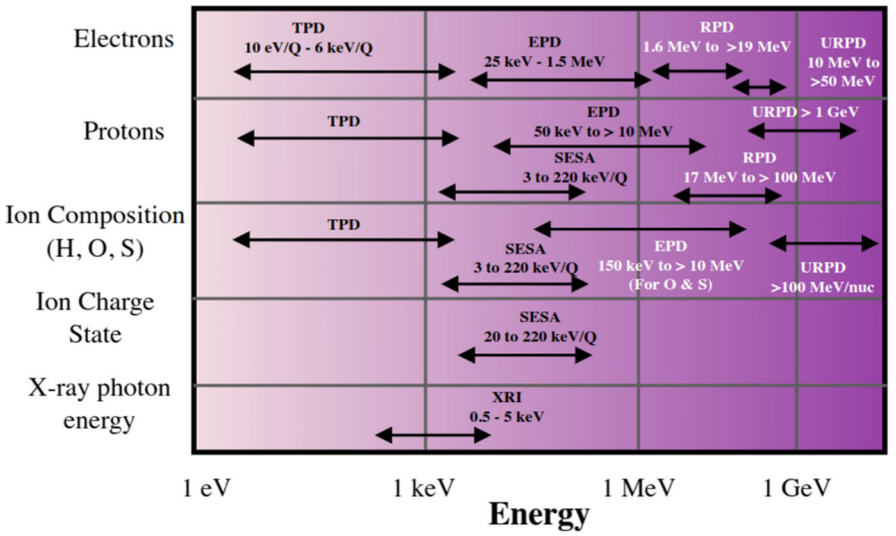

Fig. 2 Overview of on-board instrument for the COMPASS mission concept. Pix.PAN is the advanced instrument concept for the URPD payload [27]

an advanced instrument concept for the Ultra-Relativistic Particle Detector (**URPD**), whose design and expected performance are further elaborated upon in this article. To successfully address the science goals/requirements outlined above, its instrument must specify the performance criteria outlined in Section 2.

2 Instrument performance requirements

The Ultra-relativistic Particle Detector of COMPASS has the challenging task to measure the energy, direction, time, and composition of the most energetic particles that can be trapped at Jupiter, covering electrons in the range of 10 MeV to >1 GeV, protons and ions (in particular oxygen and sulfur ions) from 100 MeV/nuc to few GeV/nuc. Detectors that measure particles of such energies (or even higher) and a large range of ion masses operate routinely in the near-Earth geospace and usually target the GCR spectrum. The latter comprises very low fluxes and varies slowly, so using slow detector electronics is sufficient. Such instruments also benefit from operations at $\approx$1 AU that allows them to use relatively large resources in terms of mass and power. Ultra-relativistic particles within the Earth's magnetosphere are also at relatively low intensity levels. At Jupiter, fluxes of electrons and ions at (ultra)relativistic energies are many orders of magnitude higher than those of cosmic rays or Earth's magnetosphere, more variable at short time scales in both intensity and composition and more complex in terms of spectral shape compared to the regular power-law shape of GCRs, as hinted by existing measurements and physical models [28]. Their distribution function has never been accurately observed. New discoveries about phenomena in this energy range are expected and thus will provide clues to acceleration processes that have never been studied in-situ.

Energetic particles above about 100 MeV/nuc for protons and ions, and electrons above about 10 MeV cannot be easily stopped, thus become "penetrating", and can interact with the detector material and produce a shower of secondary particles. Therefore they cannot be measured accurately with the energetic particle instruments used in previous space missions, e.g., the Relativistic Electron-Proton Telescope (REPT) [29] or Relativistic Proton Spectrometer (RPS) instruments [30] on the Van Allen Probes, which require that the particles stop in the detector, while complying with the strict mass and power budgets of a deep space mission. Currently, the baseline design considered for the URPD on COMPASS a modified version of RPS. It determines the energy of penetrating protons with a Cherenkov radiator up to ≈1 GeV, and for ultra-relativistic electrons up to ≈50 MeV, whereas REPT, used as a baseline for COMPASS's Relativistic Particle Detector (RPD), can also resolve heavy ions up to several 100 MeV/nuc, both satisfying the mission's measurement requirements. Jupiter's magnetic field is so strong that, within Io's orbit, it can trap >100 GeV protons, while trapped electrons of ≫100 MeV and heavy ions of ≫100 MeV/nuc are also predicted by several models [31, 32], energy ranges that cannot be covered by either RPS or REPT designs. Compared to the REPT, the RPS includes a Cherenkov system for protons which manage to penetrate all its silicon layers. This enables it to expand its energy range from an initial 400 MeV to 2 GeV. Nevertheless, it should be noted that the energy resolution is 30% at 50 MeV and increases to 100% at 2 GeV. To enhance the scientific output of COMPASS by increasing the energy coverage for electrons, protons and heavy ions, and to offer additional redundancy to the challenging measurements by REPT and RPS, the concept of a compact magnetic spectrometer with a high-resolution silicon tracker with particle identification and high-rate capabilities, the Penetrating particle ANalyzer (**PAN**), has been proposed [33]. PAN is designed to go above and beyond the current state of the art of energy range, targeting energy resolutions reaching the 20-30% level for ultra-relativistic particles. Here, Pix.PAN is an implementation of the PAN concept specifically adapted for Jupiter's radiation belt studies. It should be noted that the energy resolution goal, should be achieved within the provided payload envelope. For a Jupiter mission, this implies a power budget of 20 W, a maximum mass of 25 kg (including shielding) and an (approximate) volume of $25 \times 25 \times 25\,\mathrm{cm}^3$.

3 Pix.PAN conceptual design and simulation

Relativistic energetic particles, above about 100 MeV/nuc for protons and ions, and above about 10 MeV for electrons, cannot be easily stopped, thus becoming "penetrating". Up until now penetrating particles have not been precisely measured outside the Earth's magnetosphere, while most of the time only their integrated fluxes are available. The state-of-the-art deep space energetic particle detection technology is based on the so-called $\Delta E - E$ method, where the particle has to be stopped completely in a series of thick solid-state detector layers so that its energy (E) can be measured, while its identity is inferred by measuring the energy deposited in each layer (ΔE), which is related to the speed and the charge of the particle through the well-known Bethe stopping power formula. This method has been successfully applied in many

missions, including the CRIS instrument [34] on the ACE mission, the HET [35] instrument on Voyager 1, the CRaTER [36] instrument on LRO, the EPHIN instrument on SOHO [37] and similar instruments on the GOES series of satellites [38], and the Radiation monitor RADEM of the upcoming JUICE mission [39]. However, these instruments are not able to precisely measure penetrating particles since, as explained above, these particles can no longer be stopped by the detector. In addition, these particles start to interact strongly with the detector material, producing a shower of secondary particles which degrades substantially the energy resolution.

The same $\Delta E - E$ type of detectors have also been used in previous radiation belts missions, such as the REPT [29] or RPS instruments [30] on the Van Allen Probes, thus limiting seriously their measurement capabilities for penetrating particles in terms of energy resolution, particle identification and counting rate. Magnetic spectrometer (MS) is a proven high precision detection technology for energetic particles, and has successfully been used in large space missions (e.g., Pamela [40] and AMS-02 [41]) as well as on smaller assemblies for intermediate energies (tens/hundreds of keV to few MeV electrons) in missions like the Van Allen Probes (MagEIS instrument) and the EPD/LEMMS and MIMI/LEMMS instruments on the Galileo and Cassini missions respectively. In a MS, the momentum resolution, thus the energy resolution, has two contributions: one, related to the magnetic field (strength and length) and the tracker spatial resolution, increasing with increasing momentum; the other, due to the multiple Coulomb scattering (MCS), decreasing with increasing momentum. With appropriate instrument design, it is possible to mitigate these two effects to achieve a good energy resolution over the desired energy range.

3.1 Conceptual design and enabling technologies

Penetrating particles carry critical information to unravel the complex physical processes in planetary radiation belts and solar particle events. Additionally, their measurements have significant impact on space weather and space radiation dosimetry. To fill this critical technology gap, an instrument concept based on a compact magnetic spectrometer and advanced silicon tracker technology called Penetrating Particle Analyzer (PAN) [33] was proposed, in the context of deep space application, with limited weight, dimension and power budget, but with high performance that will allow for ground-breaking measurements. A magnetic spectrometer measures the rigidity (momentum over charge p/Z) of a charged particle through its trajectory bending in a magnetic field, which then can be used to derive the momentum and energy if the charge (Z) of the particle, can be independently identified.

An international consortium with physicists from the Czech Republic (the CTU and UWB groups), Italy (INFN, Perugia Section) and University of Geneva was created to pursue its technology development. A 3-year H2020 grant [42] was approved to develop a technology demonstrator, called Mini.PAN. Development on this demonstrator greatly aided in the understanding of its design weaknesses/strength. Its design strengths (such as the mechanical compactness, high rate capability of the Pixel sub-detectors and readout system) inspired the proposed Pix.PAN instrument for the

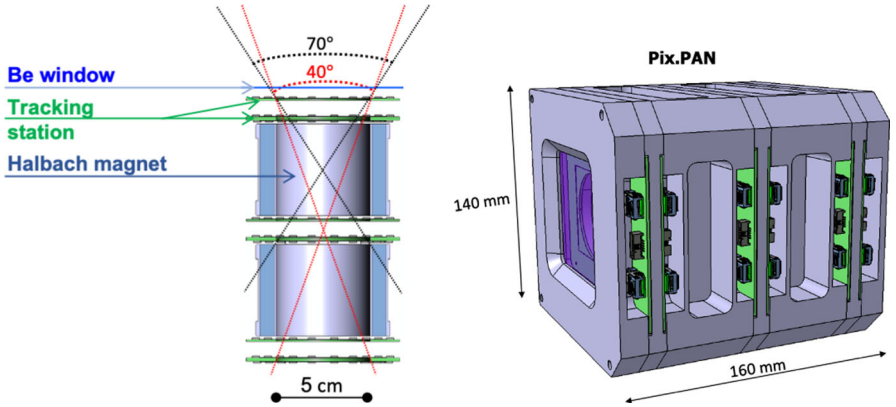

Fig. 3 **a)** A sketch of the spectrometer layout of Pix.PAN key components, showing the two magnet sectors and three tracking stations. **b)** Preliminary design of the mechanical structure of the Pix.PAN spectrometer, excluding shielding and radiator material

COMPASS mission. The baseline layout of Pix.PAN is shown in Fig. 3a. It is a cylindrical magnetic spectrometer with two Halbach-array magnet sectors of 5 cm in diameter, each providing a dipole field of ∼0.4 Tesla. The magnets are sandwiched between three tracking stations, each composed of two tracking layers 1 cm apart, to measure both the particle bending angle through each magnet, as well as its bending radius through the full spectrometer. To satisfy the performance specifications of URPD, in particular the extreme high hit rates (up to ≈60 MHz/cm^2) and the harsh operating environment, the tracking stations will be implemented with hybrid pixel detector read out by the latest version of the widely used, both on ground-based experiment and in space, Medipix/Timepix series of readout ASICs [43], the Timepix4 [44]. Not only can the Timepix4-based pixel detectors provide excellent tracking performance under high rate and hostile operating conditions, they can also provide good timing and particle charge measurements for particle identification.

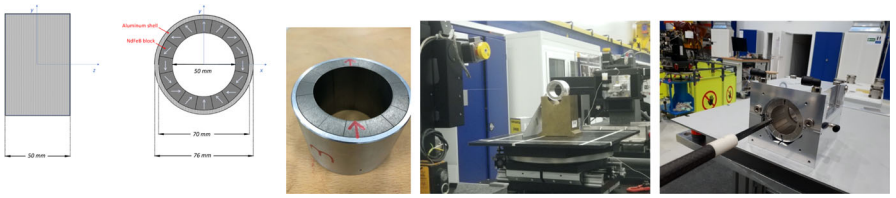

Fig. 4 The Mini.PAN magnets: **a)** Design sketch; **b)** Magnet prototype; **c)** Single magnet under integrated magnetic field measurement with stretched wire at CERN; **d)** 2-magnet assembly under 3D mapping of the magnetic field with Hall probe at CERN

3.1.1 Magnets

In the framework of Mini.PAN, the Halbach-array magnet sectors with NdFeB permanent magnet blocs have been designed, produced, measured and assembled (Fig. 4). The design requirements are mostly satisfied. The magnetic field strength along the z-axis of the instrument is expected to be as shown in Fig. 5. The figure shows that the stray field is less than 1 mT beyond 70 mm of the instrument openings (or 150 mm from the instrument center). The weight of each magnet is 0.8 kg, for a total of about 1.6 kg.

The demagnetization of permanent magnets by high doses of radiation have been studied by many experiments (for a review see [45] or [46]). The degree of demagnetization depends both on the radiation (particle type, energy and dose), the magnet itself (material, dimension, manufacturer, preparation, etc.) and the operation temperature. At the level of 100-200 krad, SmCo permanent magnets would not be demagnetized. Even with NdFeB magnets the radiation situation of Pix.PAN is manageable since:

- the total dose on the magnets behind the exterior instrument shielding is due to MeV electrons, which are expected to cause much less demagnetization than high energy protons and ions. According to one measurement [47] a magnetic flux loss of 0.5% is expected after a dose of $\approx 10^{15} \frac{\text{electrons}}{\text{cm}^2}$ of 17 MeV electrons, which is above the electron dose expected for Pix.PAN.
- the operational temperature of the magnets of Pix.PAN is expected to be well below 0°C, which can substantially reduce the effect of radiation damage [48].
- shielding strategy can be optimized to minimize the demagnetization effect

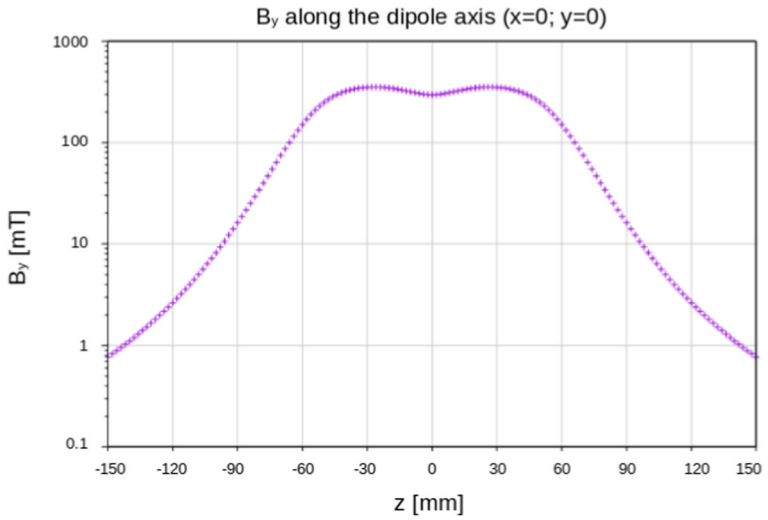

Fig. 5 Magnetic field along the z-axis for the Mini.PAN demonstrator (effectively equivalent for the Pix.PAN instrument). '0 mm' refers to centre of the instrument between the magnets

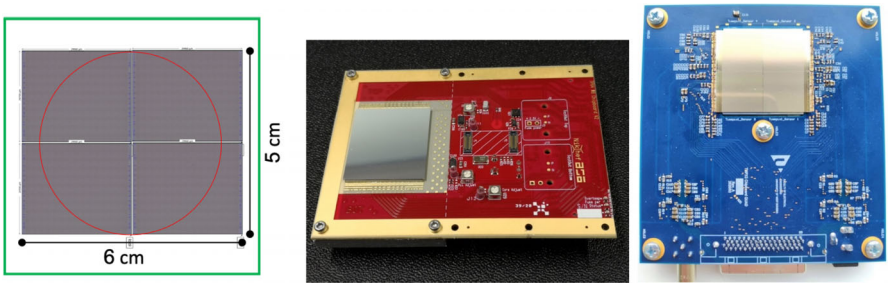

Fig. 6 **a)** Area of the Timepix4 quad assembly of a Pix.PAN tracking layer. The gap between a 2x1 sensor is about $55\mu m$. **b)** Photo of a single Timepix4 assembly with a $300\mu m$ silicon pixel detector. **c)** Photo of the Mini.PAN Timepix3 quad assembly prototype

If it is necessary to use SmCo magnets[2], due to their ∼20% lower magnetic field compared to NdFeB ones, the magnets will need to be bigger to achieve the same bending power. As a result, the weight of the 2-magnet system will be increased by about 1 kg, to about 2.6 kg (excluding the impact on the mass of the Pix.PAN encasing).

3.1.2 Tracker

The bending of a charged particle due to the magnetic field is measured by a tracker: a series of position sensitive detectors placed along the track of the particle. The tracker of the Pix.PAN instrument consists of three tracking stations, each composed of two tracking layers. Silicon strip or pixel detectors have been widely used in nuclear and particle physics experiments, as well as in space (e.g., PAMELA and AMS). Within the context of Mini.PAN, silicon strip detectors are used for the tracker design. However, during the strongest solar particle events, and within planetary radiation belts, it is very likely that pile-up (more than one particle entering the same detection element at the same time) as well as readout saturation will occur. To cope with this anticipated problem, the Mini.PAN consortium has investigated using the advanced high-rate active hybrid silicon pixel sensor technology developed by the Medipix collaborations [49], of which both the Geneva and CTU groups are members. In this context the CTU and University of West Bohemia (UWB) groups developed a protoype pixel module (Fig. 6a) consisting of four Timepix3 ASICs [50] arranged in two rows bonded to a 300 μm thick silicon pixel detector with 262,144 pixels of 55 μm pitch, covering a total area of 8 cm^2, about 20% of the Mini.PAN acceptance. The main concern of using the pixel technology in deep space is the power consumption due to the large numbers of active pixels in the sensor. The Czech groups (within the PAN consortium) have investigated the performance of Timepix3 with different operational parameters providing means of reducing the power consumption by a factor of four without compromising the performance of Mini.PAN [51]. The Timepix3 quad modules have been successfully tested individually and integrated into the Mini.PAN

[2] We are referring to the scenario where the environmental requirements for the NdFeB cannot be satisfied during the course of the mission.

spectrometer built by the Geneva group in the CERN test beam facilities (Fig. 6c). Due to the high-rate environment of Jupiter's radiation belts, silicon Hybrid Pixel Sensors based on the Timepix4 readout ASIC will be used for Pix.PAN (as shown in Fig. 6b).

Timepix is a series of hybrid pixel detector (HPD) readout ASIC developed by the Medipix2 collaboration led by CERN since 1999, and has been widely used in particle physics, nuclear physics, medical physics, and in space (for a review of Timepix space application see [52]). Recently, a TimePix based radiation monitoring system, HERA [53], was launched on Artemis 1 on November 16th 2022. Timepix4 [44] is the 4th generation of the ASIC produced and validated in 2021. The Pix.PAN tracking layer consists of silicon pixel detector readout by 2x2 Timepix4. The Timepix4 chip measures 29.96x24.7 mm^2, therefore the quad assembly can readout a silicon pixel detector up to 60x50 mm^2 in size, sufficient to cover the sensitive area of the spectrometer, as shown in the left panel of Fig. 6. Note that Timepix3 quad assembly has been successfully produced for Mini.PAN, as shown in the right panel of Fig. 6.

Timepix4 is a large area pixel detector readout chip with high rate capability, up to a hit rate of 358 MHz/cm^2. Each ASIC has 512×448 readout cells with 55 μm bump bonding pitch. In data-driven mode it has been demonstrated to operate with a threshold of 800 electrons [44], which is about 1/14 of electron-hole pairs produced by a minimum ionizing particle (MIP) in 150 μm of silicon. The energy resolution is ≈1 keV, corresponding to about 1.7% for the most probable energy loss by a MIP in 150 μm of silicon. One important feature of the ASIC, as its name indicates, is that it can provide a timestamp in 195 ps bins, allowing to use the tracker also as a Time-Of-Flight (TOF) detector, an additional handle for particle identification in Pix.PAN. The tracking layers will also measure the charge number (Z) of the particles using the dE/dx method thanks to the full analog readout capability of Timepix4.

Therefore, thanks to the powerful functionalities of Timepix4 the Pix.PAN instrument will have only one type of sensor technology, which makes it simple and robust to operate. There are also two important features: no trigger device is needed since Timepix4 uses a data-driven readout scheme, and the readout is purely digital since the ADC and TDC are fully integrated in Timepix4.

Silicon HPDs have been operated successfully in high radiation environment such as in collider experiments at the LHC at CERN, which is harsher than the 100 krad expected for Pix.PAN. Radiation induced single event upset effects can be mitigated by periodically refreshing the registers of the ASIC. The full configuration matrix of Timepix4 can be updated within 100 ms.

3.1.3 Silicon pixel detector geometry and connection scheme to Timepix4

The position resolution of a silicon pixel detector is mainly defined by the pixel size, also called pitch. In the case of a magnetic spectrometer the position resolution requirement is more stringent in the bending plane (perpendicular to the field lines) than in the non-bending plane since the energy resolution is directly linked to the precision of measuring the bending radius. To reach the 20-30% energy resolution of ultra-relativistic particles required for URPD, a position resolution of 3-5μm is needed, which can be provided with a pixel pitch of ≈10-17 μm, but on the bending direction only (see Section 3.2.1). The pixel pitch on the non-bending direction can

be larger, up to the extent that the increased total capacitance of the "long pixel" will not degrade substantially the noise performance of the detector. The current estimate is that Timepix4 can still perform very well with a long pixel of 13.75 μm$\times$1760 μm, which is expected to substantially reduce the power consumption of the system (see Section 4.1.3).

3.2 Expected performance

3.2.1 Energy measurement

The energy resolution of the spectrometer is determined by the magnetic field strength, the path length of the particle in the magnetic field, and two key parameters of the tracker: the position resolution and the thickness of the tracking layer. Since the resolution depends on the path length of the particle in the magnetic field, particles traversing more magnet sectors will have better resolution, but with a reduced geometrical acceptance. The PAN design allows to compensate the worsening of the energy resolution at low particle energies through increased statistics: for high flux particles full passage events can be used to profit from the best energy resolution, while for low flux events the measurement precision is dominated by statistics, so accepting large number of short passage events can bring significant improvement. The geometrical acceptance of the Pix.PAN demonstrator layout, with two magnet sectors of 5 cm in both length and diameter, are about two or six cm^{2}sr for particles passing two or one magnet sectors, respectively. The corresponding opening angles are about 40° or 70°, as shown in Fig. 3.

The energy resolution of the spectrometer can be analytically estimated with the Gluckstern formulas [54], which shows that a resolution at the level of 10% can be achieved for electrons in the energy range of 10 MeV-1 GeV, and at the level of 25% for protons from ~100 MeV to a few GeV. Recently, we have implemented the Pix.PAN instrument in the Geant4 particle detector simulation toolkit [55] to trace the particles through the instrument, fully taking into account the effects of the particle interactions within the detector. We have performed the analysis with Geant4 10.7.2 with the EM physics package *emstandard_opt0* and decay physics package enabled. The interacting positions of the particle at the tracker layers are then fed into the GenFit package [56], using the Kalman filter, to reconstruct the particle track in the magnetic field.

To derive the energy resolution, 10^5 particles were generated at z=−120 mm with a random deviation of ±1 mm in the xy-plane. At generation, they only have the p_z component. 26 initial kinetic energy points were simulated to fully study the energy range of interest. These are (in units of MeV): 10, 20, 50, 100, 200, 300, 400, 500, 600, 700, 800, 900, 1000, 1500, 2000, 2500, 3000, 3500, 4000, 4500, 5000, 6000, 7000, 8000, 9000, 10000. The energy resolution after reconstruction with GenFit is defined as the width of the residual distribution R_{ene}

$$R_{ene} = \frac{E_{rec} - E_{true}}{E_{true}} = \frac{\Delta E}{E_{true}} \tag{1}$$

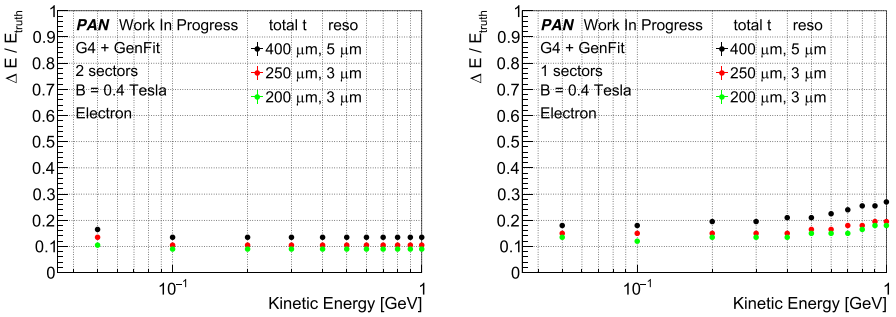

Fig. 7 Energy resolution vs. energy for electrons passing two (**a**) and one (**b**) magnet sector(s), from 10 MeV to 1 GeV

where about 68% (1σ) of the events are contained. No specific event selection is applied. Hits in each tracker layer, that are used for the fit, are taken from the average coordinate of all the Geant4 steps in that layer.

The energy resolution of Pix.PAN with the nominal magnet system design and for three configurations of the tracker position resolution and the tracking layer thickness is shown in Figs. 7 and 8 for electron and proton respectively, for particles passing two (left panels) or one (right panels) sectors. Currently, the configuration of 400 μm thickness with 5 μm position resolution (black points in the plots) can be easily achieved, while the configuration of 200 μm thickness with 3 μm position resolution (green points) requires more advanced pixel detector layout and connection scheme. From these figures, the expected energy resolution for particles traversing two (one) sectors <12% (<20%) for electrons with energies from 10 meV − 1 GeV, and of <35% (<40%) for protons of ≈200 MeV to a few GeV. We note that Pix.PAN would have the same detection characteristics for positrons and antiporotons. Trapped anti-particles in a magnetosphere result from particle-radiation material interactions. They have been detected at Earth, and are expected to be more abundant at Jupiter due to a variety of radiation-material interactions taking place in the system [57, 58].

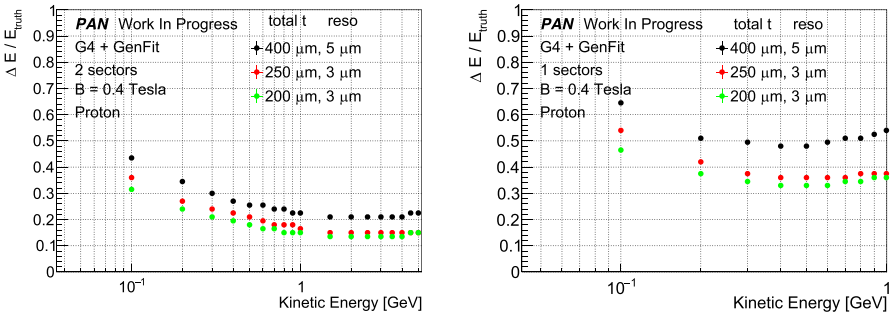

Fig. 8 Energy resolution vs. energy for proton passing two (**a**) and one (**b**) magnet sector(s), from 100 MeV to 5 GeV

The performance with the nominal configuration is already sufficient for the key requirements of URPD on electron and proton. The more "cutting edge" tracking layer configuration of 200 μm thickness with 3 μm position resolution can be achieved by using with thin pixel detector (150 μm thick) with "long" pixels of 13.75 μm pitch bonded to a Timepix4 ASIC thinned to 50 μm with through-silicon via (TSV) connectivity.

There are indications that the ions in Jupiter's inner radiation belts are mainly partially ionized oxygen and sulfur ions [59]. The energy resolution for these ions will be substantially worse than that of electrons and protons since they have high rigidities for a given kinetic energy due to their higher mass and low charge number. From the Gluckstern formulas, it is estimated that in the case of singly charged oxygen and sulfur ions, energy resolution at the level of 50-60% can only be achieved for particles passing two magnet sectors and with a tracker that has a position resolution of 3 μm. For oxygen and sulfur this is in the energy range of ≈30 MeV/n to ≈350 MeV/n and ≈20 MeV/n to ≈100 MeV/n respectively. For ions with higher ionization states the energy resolution will be better due to their lower rigidities. The preliminary Geant4+GenFit evaluation for singly charged and fully ionized heavy ions are shown in Fig. 9. As expected, the energy resolution for singly ionized ions are worse than protons, electrons, and fully ionized ions. The reconstructed energy distribution in the

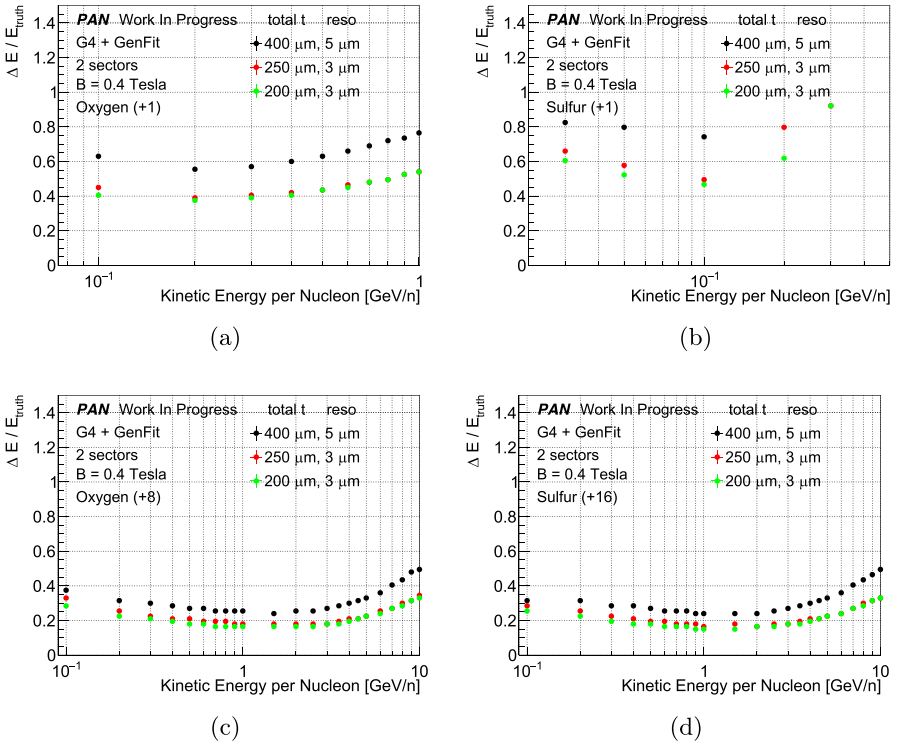

Fig. 9 Energy resolution vs. energy for singly (top) and fully (bottom) ionized oxygen (**a** and **c**) and sulfur (**b** and **d**) ions passing two magnet sectors as a function of the kinetic energy per nucleon

energy range above 100 MeV/n for the singly ionized sulfur (see Fig. 9b) for a 250 μm thickness case is not consistent with the 200 μm thickness case. This results from the, currently, incomplete fitting algorithm which (at the time of writing) is still being investigated.

3.2.2 High rate capability

It is known that the main particle flux within Jupiter's radiation belts are electrons and protons[3]. The hit rates expected for Pix.PAN on board a Jupiter radiation belts mission are estimated from the electron and proton fluxes from the physics-based Salammbo model [31, 32, 61]. Given that in the baseline design Pix.PAN will use a 3mm Be window, which will block out electrons below 1 MeV and protons below 20 MeV, a maximum total (electron>1 MeV and proton >20 MeV) integral omnidirectional flux of $1.4 \times 10^8 cm^2 s^{-1}$ is estimated at L[4]=1.59, of which $8 \times 10^7 cm^2 s^{-1}$ is from electron and $6 \times 10^7 cm^2 s^{-1}$ is from proton. Assuming an isotropic flux the maximum integral flux is then $1.1 \times 10^7 cm^2 s^{-1}$.

The first two tracking layers of the first tracker station will have the highest hit rate. With a Geometrical Factor of 4 cm^2sr they are expected to have a maximum hit rate of 44 $\frac{\text{MHz}}{\text{cm}^2}$, which is still about eight times below the hit rate limit of Timepix4 (360 $\frac{\text{MHz}}{\text{cm}^2}$). The maximum hit rate of other tracking layers will be about three times lower because electrons below 5 MeV will be swept aside by the magnetic field.

3.2.3 Particle identification

The Pix.PAN instrument has 3 sets of measurements that can be used to identify the particle: the bending direction, the time of flight, and energy depositions in the tracking layers.

In the absence of positrons and antiprotons, a reasonable assumption in Jupiter's radiation belts, the identification of electrons is trivial, since it bends in the opposite direction in the instrument to those of proton and ions. There are also extra handles to separate electron from proton and ions: the energy deposited in the tracking layers (dE/dx) and the time of flight (TOF).

As shown in the left panel of Fig. 10, the difference in the average dE/dx of electrons up to 600 MeV is about 66 keV below that of proton. Assuming a reasonable 20% resolution on the average dE/dx, this measurement can be used to separate electron up to 600 MeV from protons with about 5σ significance. Note that for particles traversing two magnet sectors six independent dE/dx measurements are available, while for those traversing one magnet sectors four are available.

The right panel of Fig. 10 shows the expected time of flight for electron and proton as a function of rigidity. For a particle traversing two magnet sectors, for which the time is measured at six points, the resolution on the average of these six measurements $<t_6>$

[3] There are also substantial contributions of sulfur and oxygen. Their fluxes are comparable to those of protons up to 10 MeV [60].

[4] L is the distance in planetary radii between the center of a planet and the apex of a magnetic field line and is commonly used to organize particle distributions in planetary radiation belts.

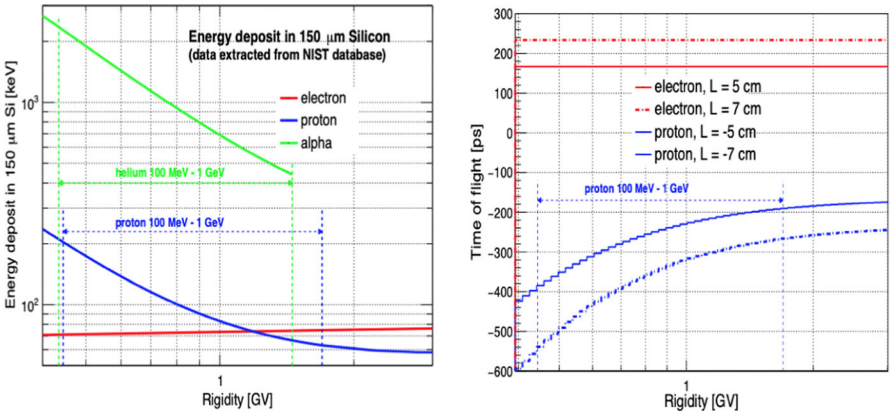

Fig. 10 **a)** Average ΔE (energy loss) in $150\mu m$ silicon for electron, proton and alpha particles vs rigidity; **b)** Time-of-flight for particles traversing two or one magnet sector(s) for electron and proton vs rigidity

is about 82 ps, since the Timepix4 can provide a timestamp with $<$200 ps precision. At a rigidity of 440 MV, which corresponds to an electron of 440 MeV or a proton of 100 MeV, the difference in $<t_6>$ between electron and proton is 672 ps, leading to a separation power of $\approx 5.8\sigma$. Applying the same calculation to a rigidity of 1 GV particle (1 GeV electron or 455 MeV proton) the separation power is $\approx 4.4\sigma$. In the case where a particle traverses only one magnet sector, the number of time measurement is four and resolution on their average $<t4>$ degrades to $200/\sqrt{4} = 100$ ps, and the separation power is reduced to $\approx 2.6\sigma$ and $\approx 2\sigma$, for particles with a rigidity of 444 MV and 1 GV, respectively.

The main method for ion identification is through the determination of its charge (Z) by measuring the energy deposited in the tracking layers, using the "dE/dx" method, which depends on the speed of the particle ($\beta\gamma$), and scales with Z^2. For particles traversing two magnet sectors six independent measurements are available, while for those traversing one magnet sectors four are available. The energy deposit of highly ionized O and S ions are larger than the saturation point of Timepix4 but since their energy deposits spread over many pixels they can still be separated by using the cluster size to correct the saturation effect [62]. In addition, the TOF information can be used as an additional handle to identify ions, in particular the singly ionized O and S ions in the energy ranges that has 50%-60% energy resolution.

3.3 TRL evaluation

All the detector components of Pix.PAN, the Halbach-array magnets and Timepix silicon hybrid active pixel sensor assembly have been used in space before, the same as the magnetic spectrometer measurement method. The actual implementation of the Pix.PAN is new, but prototypes magnets and quad Timepix assembly have been produced and tested in the Mini.PAN program. Although new prototypes with Timepix4

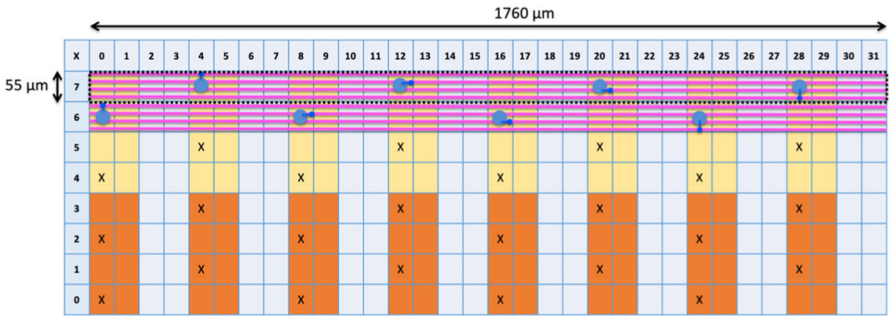

Fig. 11 Corner of the Pix.PAN pixel sensor showing the pixel size (magenta square), some of the double metal connection between the pixels and the bonding pads of Timepix4 (cyan circle), with other connection locations indicated (black crosses)

need to be produced and tested we still can consider the TRL of Pix.PAN at five or six.

There are two key technology R&Ds that are needed to be addressed:

- Silicon pixel detector geometry and connection scheme to Timepix4 optimized for the Pix.PAN application for COMPASS;
- Real time data processing with Machine Learning algorithm implemented on AI capable hardware.

3.3.1 Silicon pixel detector geometry and connection scheme to Timepix4

As discussed in Section 3.1, a key feature of the Pix.PAN instrument is the silicon pixel sensor geometry that is adapted for the specific spectrometer application. To achieve the required position resolution with a power budget suitable for deep space instrument, and within the current manufacturing capabilities, the Pix.PAN team has converged on a sensor with "long pixels" of $13.75\,\mu\text{m} \times 1760\,\mu\text{m}$. To connect this non-standard pixel detector to the $55\,\mu\text{m} \times 55\,\mu\text{m}$ square readout cells of Timepix4 a specific "pitch adapter" will be integrated into the pixel sensor using a "double metal" structure. The preliminary pixel geometry and connection scheme developed together with the Finnish company ADVACAM OY[5] is shown in Fig. 11. With this connection scheme not only 7/8 of analog power is saved, part of the digital power can also be saved since the number of ADC and clock generators will be reduced. Since the Timepix4 requires the top and bottom sides to be free for wire-bonding, a Pix.PAN sensor can cover two ASICs, therefore a tracking "quad" layer contains 2-pixel sensors read out by four Timepix4 ASICs, as shown in Fig. 12c. The total number of pixels in a layer is 114,688, therefore 688,128 for the whole instrument.

This sensor geometry needs to be first validated with the Timepix4 simulation in terms of noise performance. Then sensor prototypes need to be produced to evaluate the energy resolution achievable with various sensor thickness, which affects both the signal to noise ratio, and the multiple scattering effect. To minimize dead space the

[5] ADVACAM is specialized in semiconductor sensor production an packaging. They also develop radiation (imaging) detectors.

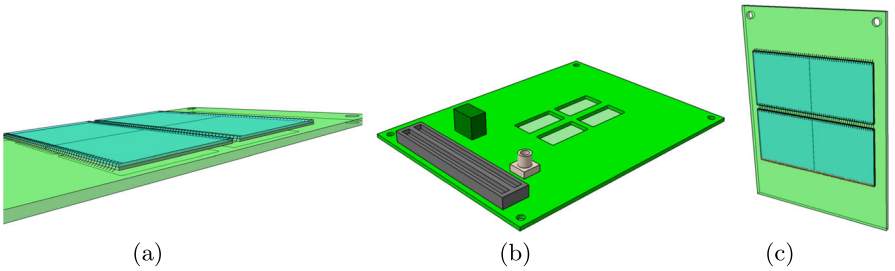

Fig. 12 Some preliminary drawings of the Pix.PAN pixel quad layers. **a)** and **c)** Front view of a the tracker layer. **b)** Rear view of the tracker layer with cutouts underneath the sensor to reduce the material the particle traverses through. A simplified set of components can also be seen which supply power and transmit data. The current design implementation uses wire bonds for high rates. As a result, due to the bonds, there will be gap within the Timepix4 quad (see **c)**)

advanced interconnect TSV technology can be used to connect the ASICs to a carrier PCB, which will have cut out areas under the ASICs to minimize dead material on the passage of the particles. Note that TSV connectivity has already been foreseen in the Timepix4 design and its TSV processing and assembly procedures are currently being developed by several institutions, including the Fraunhofer Institute for Reliability and Microintegration (IZM) in Germany. Given its complexity the quad assembly will need to be validated with prototypes and space qualified, for both mechanical and thermal aspects.

3.3.2 Tracking quad layer

A key hardware task for Pix.PAN is to develop the tracking quad layer, taking into account the science and space requirement in terms of mounting precision, minimal material in the sensitive space, low weight and mechanical and thermal stability. Similar objects had been successfully built in the context of Mini.PAN (although Timepix3 technology was used instead). At the time of writing, the production for a Timepix4-base quad is underway. Figure 12 shows some simple sketches of the Pix.PAN quad layers. The development (by members of the PAN consortium) will be led by the Czech teams based on the experience on the Timepix3 quad layer, with the participation of the Geneva group to ensure that the science and operation requirements are met, as well as a smooth integration into the tracking stations (also referred to as "tracker modules"). In the first phase two quad layers, one with 300 μm sensors and another with 150 μm sensors will be produced and validated, followed by a series production to produce up to 10 quad layers in total for the construction of tracking stations for the instrument prototype development.

3.3.3 Real time data processing

For an implementation on a Jupiter mission the real-time on-board processing of the Pix.PAN raw data is mandatory. As explained previously the data processing of a MS, including the track reconstruction and particle identification, are well understood, but

typically implemented as software algorithms running on computer clusters where power consumption is not the main concern. For the COMPASS application where the required data output is well-defined for the science objectives, the data processing can be optimized in terms of precision vs power consumption, using more advanced approaches such as Machine Learning based algorithms, which are particularly suitable for the multivariate problems of tracking and particle identification, and can profit from the emerging AI capable electronics hardware, such as the Xilinx Kintex Ultrascale XQRKU060 Space-Grade FPGA. The expected data rates are further discussed in Section 4.1.6.

4 Pix.PAN interface requirement definition

4.1 Operational environment of Pix.PAN

4.1.1 Survival temperature

SmCo magnets can operate in a very large temperature range. NdFeB magnets undergo a spin reorientation at low temperature resulting in a decrease of magnetic field. This transition happens at temperature around -135°C. The maximum working temperature of NdFeB magnets depend on the manufacturing grade and can vary between 80°C to about 230°C. For example the magnet sectors produced for Mini.PAN uses the N48H grade magnets, which has maximum working temperature of 100°C. The Timepix hybrid pixel detector has been shown to work in low temperature, down to -135°C [63] (although a repeat with the latest generations) and in vacuum from -20°C to 80°C [64]. It is therefore likely that the survival temperature of Pix.PAN will depend more on structural consideration than the functioning components of the device. For this reason, a survival temperature range of -70°C to 70°C is proposed.

4.1.2 Temperature operation

Both the magnets and the tracker perform better at low temperature in terms of noise and resolution. Since the magnet is thermally isolated from the tracker, a relatively low operation temperature, e.g. -30°C can be envisioned. How low the operation temperature on the pixel detector assembly can be achieved will depend on the cooling system to remove about 20W of power expected. The aim is to operate the tracker below -10°C. As a matter of fact, the temperature stability is more important than the absolute temperature value (as it impacts the tracker mechanical stability due to thermal expansion/contraction). For Pix.PAN the requirement is $< \pm 2$°C per hour during science data taking periods.

4.1.3 Power consumption

The power management of the Timepix4 is highly flexible. When running at the full capacity it consumes about 0.5 W cm^{-2}, which would lead to 60 W for the full instrument. However, each readout cell can be individually switched on and off,

allowing the optimization of power for specific use case. In the case of Pix.PAN since good position resolution is only needed in the bending plane, "long" pixels instead of square pixels detector can be used. For a sensor with a pixel size $13.75 \times 1760\,\mu m^2$ as proposed above, the number of readout cells is reduced by a factor of 8, thus reducing the total power consumption to 25 W. Furthermore, the number of readout links can be between 2 and 16, and the readout clock can be run at different frequencies, both can be optimized according to the application case to reduce the power consumption. With more power savings from the digital and analog front end, it is possible to fit the average power consumption of the device to a 20 W power budget. This can be achieved through, e.g., the configuration settings (such as a "low power" mode) or choice of clock speed. For TimePix3, these studies were already performed [51]. Similar studies for Timepix4 are currently underway. Note that the power consumption of the device can be dynamically managed according to the orbit and science need since it takes less than 100 ms to fully reconfigure the ASICs. Additional power to cool and perform the on-board data processing is expected to be on the COMPASS platform side. For the latter, this may add an additional peak power of 5 W, depending on peak particle rate. Facing deep space and assuming a platform temperature of 0 °C, Pix.PAN does not require active cooling.

4.1.4 Weight

As mentioned in Section 3.1, the two NdFeB magnet sectors in the Pix.PAN weigh about 1.6 kg, and if it is necessary to use SmCo magnets it will increase to about 2.6 kg. The tracking layers are very light since they consist of only the pixel detector ($150 - 200\,\mu m$), the Timepix4 ASIC ($50\,\mu m$ thick) and supporting PCB. The supporting structure with thermal connection to radiators and cables will add a few kg. It is expected to total weight excluding the shielding and radiators should fit within an 8 kg mass budget.

4.1.5 Radiation dose

A dedicated Pix.PAN model with shielding is implemented in Geant4 to characterize the instrument and simulate the dose for each tracking layers. The Pix.PAN spectrometer is implemented as shown in Fig. 13a, with two magnet sectors and six sensor layers (Fig. 13b). The thickness of the pixel sensor is $300\,\mu m$ while that of the ASIC is $100\,\mu m$. The two cylindrical NdFeB permanent magnet sectors provide a dipole field of 0.4 T. Each sector has a tube-like shape with an inner radius of 25 mm and an outer radius of 35 mm, made from 16 segments that are encased in an Aluminum shell of 3 mm thick. The shielding is modeled as a hollow cuboid of $101 \times 101 \times 150\,mm^3$, 5 mm thick, with an opening at one end (Fig. 13 right). It is composed of tungsten and weighing about 6.4 kg. At the opening a 3 mm beryllium shield is placed to block low energy electrons below ≈800 keV. Note that the large mechanical support shown in the right panel of Fig. 3 is not included, which will provide extra shielding.

The radiation dose is evaluated for Sensor #0 (nearest to the opening) and Sensor #5 (last layer). First, in order to understand effects of particle types, particle energy, geometry, and magnetic field, isotropically distributed protons and electrons are injected

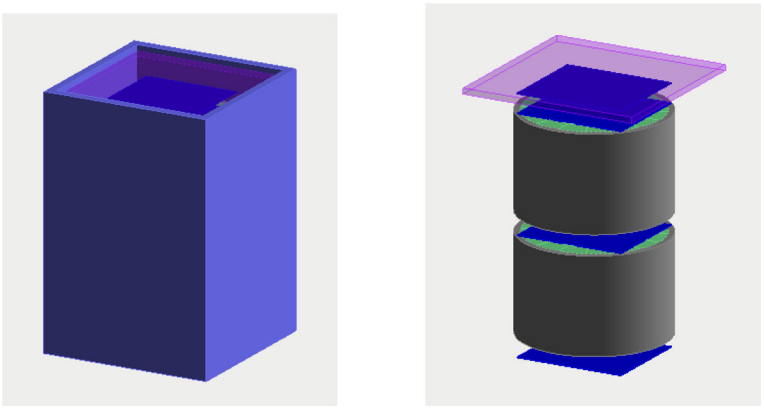

(a) (b)

Fig. 13 Visualization of the (preliminary) Pix.PAN mass model in GEANT4 with (**a**) and without (**b**) shielding. There are six blue layers, each denoting a Timepix4 sensor. These are numbered from 0 (near the opening/front) to five (near the back)

from a circular plane with a radius of 2 cm at the front and back of the instrument (separate simulation batches). For each simulation scenario the magnetic field in the instrument has been enabled/disabled.

Figure 14 shows the average proton dose as a function of the primary particle energy with and without the magnetic field enabled, for both front and back injections. It can be seen that irrespective of injection point, the impact of the magnetic field on protons is negligible, reflecting the fact that protons can only pass through the Be plate with energies above 20 MeV (above 80 MeV for tungsten shielding). At these energies, the proton cannot be significantly bended by the magnetic field. It shows also that Sensor #0 will have the highest dose, predominantly from protons of 20-50 MeV arriving from the front.

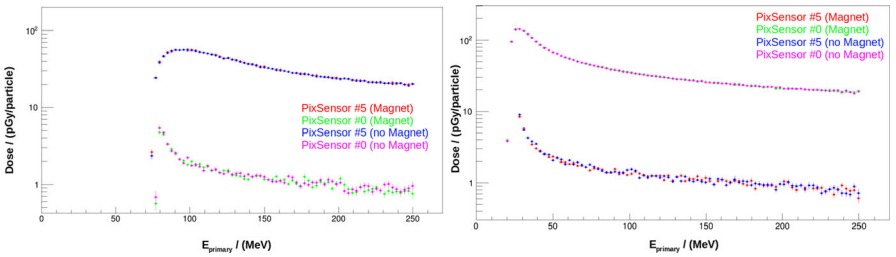

(a) (b)

Fig. 14 Comparison of the average dose for **protons** as a function of primary energy when the magnetic field is enabled and disabled, for particles injected from the front (**a**) and from the back (**b**). The "smoothed" Bragg peak for the tracker layers located furthest away from the injection point results from the energy deposit of the secondaries produced as the particle traverse through the instrument

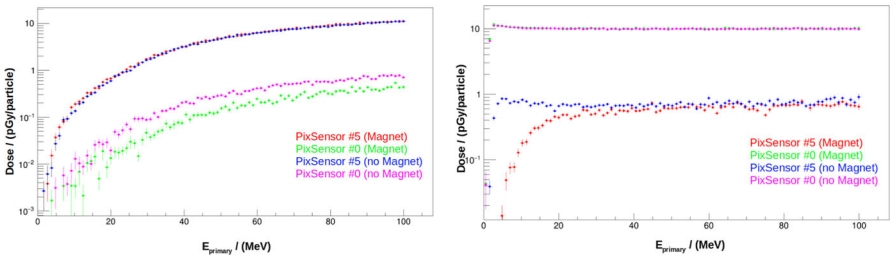

Fig. 15 Comparison of the average dose for **electrons** as a function of primary energy when the magnetic field is enabled and disabled, for particles injected from the front (left) and from the back (back)

The impact of the magnetic field effect is more evident for electrons, shown in Fig. 15, due to its lower mass. Most of the electrons below 20 MeV entering from the front will not reach Sensor #5 because of the magnet sweeping (Fig. 15 left), which will also reduce by 50% the dose on Sensor #0 from electrons entering from the back (Fig. 15 right). Taking into account the fast-falling electron spectrum at Jupiter, the highest dose is still on Sensor #0 from front entering electrons of a few MeV.

With these basic validations of the dose calculation, following successive steps towards ever increasingly realistic dose estimates are taken:

- Inject particles isotropically from a sphere covering the full instrument. A sphere of a 12.5 cm radius with Pix.PAN at its center is used.
- Use a "realistic" electron and proton input spectrum along a representative orbit at Jupiter's radiation belts. The kinetic energy spectra of electron and proton omnidirectional fluxes were computed with the ONERA JOSE-Salammbô specification model. JOSE-Salammbô employs an empirical model for L>9 and uses the Salammbô physics-based model for L<9 [65]. The electron and proton

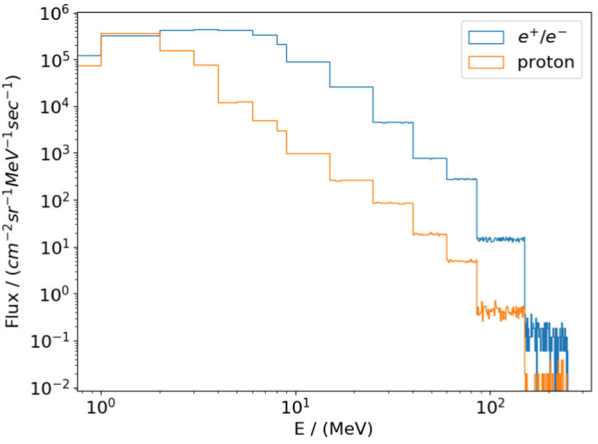

Fig. 16 Anticipated primary proton and electron flux when Pix.PAN is about 2.01 R_j from Jupiter with a latitude and longitude of 0.41 ° and 332.3 ° respectively

fluxes computed here rely on the latest version of Salammbô for L<9 [31, 32]. Figures 16 and 17 shows the electron and proton spectrum at a distance of 2.01 RJ from Jupiter with this model. At this location the electron and proton fluxes are high. For dose estimates a combined particle spectrum is randomly generated by sampling the appropriate particle energy and type. This also allows to check the spectra of secondary particles impacting on the detector elements (right panel of Figs. 16 and 17)

- Finally, the accumulated dose during the course of the full trajectory/mission can be estimated for the COMPASS mission using JOSE-Salammbo fluxes computed all along the COMPASS trajectory. The trajectory is designed in a way to satisfy both the in-situ and remote sensing observations required for the mission and to mitigate radiation. It comprises 14 elliptical orbits, with fast crossings through the belts' hazardous region, as well as a high and low latitude phase. For each point on the trajectory, 10^8 particles are injected on the sphere. Based on the input flux and injected particle number the 'equivalent time in space' is derived (i.e. 'seconds it takes for the number of particles to pass through the instrument'). As the flux varies with respect to the platform's position, it allows us to obtain the dose rate for protons and electrons as a function of the elapsed mission time. The results are shown in Fig. 18. It can be observed that overall, the electron dose rates are about 100 times higher compared to the proton dose rates, and the accumulated dose rates rise sharply towards the end of the mission when the space craft is approaching

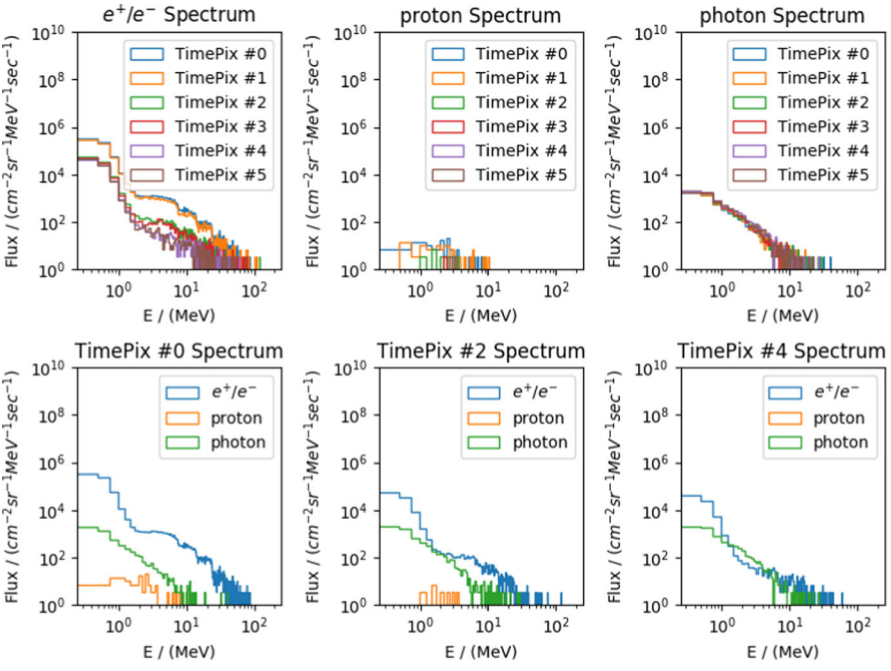

Fig. 17 Flux spectra of electrons, protons and photons inside each Timepix4 sensor. The injected energy spectra of protons/electrons is taken from Fig. 16

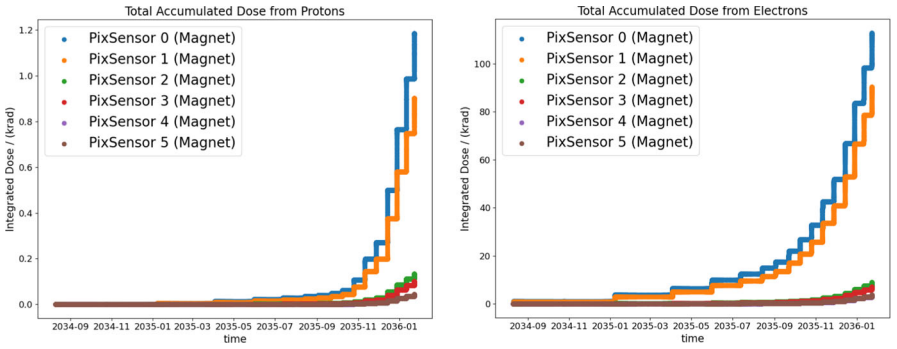

Fig. 18 Accumulated dose for each Pix.PAN sensor with the magnetic field enabled as a function of the COMPASS mission time, from electrons (**a**) and protons (**b**) flux

within 10 R_j radius to Jupiter. The total dose at the end of the mission is not larger than 120 krad, at the same order of magnitude estimated by the COMPASS mission design team. This is actually a very encouraging result as the mass model used in this evaluation does not include the mechanical support structure and any mutual shielding by the spacecraft body. We therefore anticipate the dose to be even lower, which will be quantified in the next iteration of the simulation. The fact that the radiation dose is predominantly due to MeV electrons is also a very positive since radiation damages to silicon and NdFeB magnets are expected to be smaller than compared to same total dose produced by protons and heavy ions.

4.1.6 Data processing

The data processing of a magnetic spectrometer with silicon tracker is well known and have been exercised in many ground and space based experiments, with typical algorithms for hit finding, hit pattern recognition and track fitting for the momentum measurement, and the dE/dx and TOF reconstruction for particle identification. In general data processing is done "offline", after transferring the raw data to a long term storage, although real-time track reconstruction and momentum measurement have been implemented in a few ground-based experiments, e.g., the online track trigger system SVT [66] of the CDF experiment at Fermilab, and its subsequence development FTK [67] for the ATLAS experiment at CERN, using the Associated Memory parallel lookup table method.

In the case of Pix.PAN for the URPD application real time data processing is mandatory. Each hit in the Timepix4 detectors is written in 64-bit data packages. The information includes timing, energy and associated housekeeping data. Assuming the particle flux simulated by JOSE-Salammbo at L=2, the expected raw data rate is 82.7 GB/s. By imposing a first order event selection criteria (through a sliding time window over the hits in each layer) the data rate can be reduced to 6.3 GB/s and 845 MB/s for particles passing through one and two magnet segments respectively. Two points must be noted: i) At L=2 the particle flux is highest along the orbit.

In less radiation intense regions (along the orbit) the proton and electron integral flux can reduce by about two and three orders of magnitude respectively [31, 32, 61]. ii) The study does not account for the added shielding from the mechanical structure as well as the spacecraft. This will therefore reduce the data rate even further. Nevertheless, the preliminary estimates already stress the importance/need of on-board data processing. Dedicated software tools can be written for it for quick on-board analysis. Alternatively, growing choices of ML (Machine Learning) capable hardware (FPGA and microprocessors) can be implemented. Alternatively, the data volume can be reduced at the expense of temporal resolution by only gathering it every 10 s (instead of every second). Data compression software tools may also be implemented to further reduce the transmitted data.

4.2 Interface requirements towards COMPASS instrument

At the time of writing this document, there is no clear design available for the COMPASS instrument. It is therefore not possible to provide a clear interface requirement. Nevertheless, based on the environment limitations discussed in Section 4.1, it is possible to list several minimal requirements. These are:

- COMPASS must ensure that Pix.PAN remains with an operating temperature range of -30°C to 70°C
- The Thermal control system must allow for temperatures to fluctuate within $<\pm 2$°C per hour
- COMPASS must provide 20W of power for the full payload
- COMPASS should have an available mass budget of at least 8kg (excluding Pix.PAN's external shielding)
- COMPASS must have a sufficiently powerful on-board computer for immediate data processing (this can also be included within the envelope of the Pix.PAN payload design)
- COMPASS must have an on-board data storage system for temporary high data rates which can be transmitted when the space probe is in a low radiation area

If these requirements cannot be satisfied then it can lead to a low precision (temperature instability) or even total loss (exceeding survival temperature limits) of the energy measurement. As far as the electronics are concerned, a malfunction of the power supply and back-end electronics can lead to a complete payload failure. Therefore, redundancy is needed. Finally, an unexpected data rate can lead to loss of data because of down-link rate/onboard memory limits, degrading the overall collected statistics.

5 Summary and outlook

We have presented Pix.PAN, a Timepix4-based compact magnetic spectrometer, in this white paper within the context of COMPASS, a mission concept intended to study Jupiter's radiation belts. The conceptual design, expected performance and TRL were discussed. Our studies have shown that despite the harsh radiation environment, the

instrument is capable of performing energy resolved analyses with a resolution of $<12\%$ for electrons between 10 MeV and 1 GeV. For protons the energy resolution is $<35\%$ between $\sim$200 MeV and a few GeV. Due to the timestamp precision of Timepix4, a time resolution between 82 ps and 100 ps can be achieved. Based on available flux models, we have also concluded that the readout technology hit rate design limit of $360\frac{\text{MHz}}{\text{cm}^2}$ is well beyond the expected maximum rate of $44\frac{\text{MHz}}{\text{cm}^2}$. However, our study also shows that at high radiation environments, an on-board software system is necessary to pre-process the data to reduce it from about 850 MB/s (at the point where the particle flux is highest) to an acceptable data rate level. This can be done through either smart cluster algorithms and/or AI capable hardware (FPGA and microprocessors).

Finally, we have summarized the necessary requirements for the instrument. From a thermal perspective, the instrument must operate between -30°C and 70°C with a thermal control system that allows for temperatures to fluctuate within $<\pm 2$°C. From a mass budget perspective, a minimum weight of 8 kg is needed. The instrument will also require a minimum power of 20 W.

As can be inferred from the conclusions of our study, Pix.PAN also has the capacity to be used for other space-borne missions where high energy particles and high particle rates are expected. Therefore, it can also be used for cosmic ray monitoring purposes outside Earth's magnetosphere as well as solar flare studies. Finally, Pix.PAN can also be used for human space exploration where radiation environments must be monitored for health purposes.

Author Contributions The main authors are Johannes Hulsman and Xin Wu. Johannes Hulsman is considered the primary of the two. The first draft of the manuscript was written by Johannes Hulsman and Xin Wu and all authors commented on previous versions of the manuscript.

Funding Open access funding provided by University of Geneva. We gratefully acknowledge the financial support granted by the Swiss Space Office of the State Secretariat for Education, Research and Innovation SERI to the study on the Pix.PAN instrument.

Code availability Not applicable.

Declarations

Conflicts of interest The authors declare that the research was conducted in the absence of any commercial or financial relationships that could be construed as a potential conflict of interest.

Competing interests The authors declare no competing interests.

Consent to participate Not applicable.

Consent for publication Not applicable.

References

1. Van Allen, J.A., Ludwig, G.H., Ray, E.C., McIlwain, C.E.: Observation of high intensity radiation by satellites 1958 alpha and gamma. Jet Propulsion. **28** (1958). https://doi.org/10.2514/8.7396
2. Hess, W.N.: Energetic particles in the Inner Van Allen Belt. Space Sci. Rev. **1**(2), 278–312 (1962). https://doi.org/10.1007/BF00240580
3. Mauk, B.: Comparative investigation of the energetic ion spectra comprising the magnetospheric ring currents of the solar system. J. Geophys. Res.: Space Physics. **119** (2014). https://doi.org/10.1002/2014JA020392
4. Mauk, B., Fox, N.: Electron radiation belts of the solar system. Journal of Geophysical Research. **115** (2010). https://doi.org/10.1029/2010JA015660
5. Miller, M.W., Kaufman, G.E., Maillie, H.D.: In: Sneath, P.H.A. (ed.) Pioneer 10 and 11 Jovian Encounters: radiation dose and biological lethality, pp. 195–200. De Gruyter, Berlin, Boston (2022). https://doi.org/10.1515/9783112516843-022
6. Fillius, W., Ip, W.H., McIlwain, C.E.: Trapped radiation belts of saturn: first look. Science. **207**(4429), 425–431 (1980). Accessed 22 Sep 2022
7. Roussos, E., Allanson, O., André, N., Bertucci, B., Branduardi-Raymont, G., Clark, G., Dialynas, K., Dandouras, I., Desai, R.T., Futaana, Y., Gkioulidou, M., Jones, G.H., Kollmann, P., Kotova, A., Kronberg, E.A., Krupp, N., Murakami, G., Nénon, Q., Nordheim, T., Palmaerts, B., Plainaki, C., Rae, J., Santos-Costa, D., Sarris, T., Shprits, Y., Sulaiman, A., Woodfield, E., Wu, X., Yao, Z.: The in-situ exploration of Jupiter's radiation belts. Exp. Astron. (2021). https://doi.org/10.1007/s10686-021-09801-0
8. Singer, S.F.: "radiation belt" and trapped cosmic-ray albedo. Phys. Rev. Lett. **1**, 171–173 (1958). https://doi.org/10.1103/PhysRevLett.1.171
9. Reames, D.V.: Seps: Space weather hazard in interplanetary space, pp. 101–107. American geophysical union (AGU), ??? (2001). https://doi.org/10.1029/GM125p0101
10. Li, W., Ma, Q., Thorne, R.M., Bortnik, J., Kletzing, C.A., Kurth, W.S., Hospodarsky, G.B., Nishimura, Y.: Statistical properties of plasmaspheric hiss derived from van allen probes data and their effects on radiation belt electron dynamics. J. Geophys. Res. Space Phys. **120**(5), 3393–3405 (2015). https://doi.org/10.1002/2015JA021048
11. Zhao, H., Baker, D.N., Li, X., Malaspina, D.M., Jaynes, A.N., Kanekal, S.G.: On the acceleration mechanism of ultrarelativistic electrons in the center of the outer radiation belt: A statistical study. J. Geophys. Res. Space Phys. **124**(11), 8590–8599 (2019). https://doi.org/10.1029/2019JA027111
12. Adams, E.Y., Fretz, K.A., Sr., U., Fox, N.J.: Van allen probes mission overview and discoveries to date. **33**, 173–182 (2016)
13. Millan, R., McCarthy, M., Sample, J., Smith, D., Thompson, L., Mcgaw, D., Woodger, L., Hewitt, J., Comess, M., Yando, K., Liang, A., Anderson, B., Knezek, N., Rexroad, W., Scheiman, J., Bowers, G., Halford, A., Collier, A., Clilverd, M., Hudson, M.: The balloon array for rbsp relativistic electron losses (barrel). Space Sci. Rev. **179** (2013). https://doi.org/10.1007/s11214-013-9971-z
14. Selesnick, R.S.: Cosmic ray access to jupiter's magnetosphere. Geophys. Res. Lett. **29**(9), 12–1124 (2002). https://doi.org/10.1029/2001GL014146
15. Clark, G., Kinnison, J., Kelly, D., Kollmann, P., Li, W., Jaynes, A., Blum, L., Marshall, R., Turner, D., Cohen, I., Ukhorskiy, S., Mauk, B., Roussos, E., Nénon, Q., Drozdov, S., Li, X., Woodfield, E., Dunn, W., Berland, G., Kraft, R., Williams, P., Smith, T., Sorathia, K., Sciola, A., Hospodarsky, G., Wu, X., O'Brian, P., Looper, M., Sicard, A., Santo, A., Leary, M., Haapala, A., Siddique, F., Donegan, M., Clare, B., Emmell, D., Slack, K., Wirzburger, J., Sepulveda, D., Roufberg, L., Perry, J., Schellhase, J., Pergosky, D., Able, L., O'Neill, M., Fernandes, C., Chattopadhyay, D., Bibelhauser, S., Kijewski, S., Pulkowski, J., Furrow, M.: Comprehensive Observations of Magnetospheric Particle Acceleration, Sources, and Sinks (COMPASS): a mission concept to jupiter's extreme magnetosphere to address fundamental mysteries in heliophysics. Authorea, Inc. (2023). https://doi.org/10.22541/essoar.167751608.84818747/v1

16. Roussos, E., Cohen, C., Kollmann, P., Pinto, M., Krupp, N., Gonçalves, P., Dialynas, K.: A source of very energetic oxygen located in jupiter's inner radiation belts. Sci. Adv. **8**(2), 4234 (2022). https://doi.org/10.1126/sciadv.abm4234
17. Birmingham, T.J.: Charged particle motions in the distended magnetospheres of jupiter and saturn. J. Geophys. Res. Space Phys. **87**(A9), 7421–7430 (1982). https://doi.org/10.1029/JA087iA09p07421
18. Levin, S.M., Bolton, S.J., Gulkis, S.L., Klein, M.J., Bhattacharya, B., Thorne, R.M.: Modeling jupiter's synchrotron radiation. Geophys. Res. Lett. **28**(5), 903–906 (2001). https://doi.org/10.1029/2000GL012087
19. Girard, J.N., Zarka, P., Tasse, C., Hess, S., Pater, I., Santos-Costa, D., Nenon, Q., Sicard, A., Bourdarie, S., Anderson, J., Asgekar, A., Bell, M.E., Bemmel, I., Bentum, M.J., Bernardi, G., Best, P., Bonafede, A., Breitling, F., Breton, R.P., Broderick, J.W., Brouw, W.N., Brüggen, M., Ciardi, B., Corbel, S., Corstanje, A., Gasperin, F., Geus, E., Deller, A., Duscha, S., Eislöffel, J., Falcke, H., Frieswijk, W., Garrett, M.A., Griessmeier, J.-M., Gunst, A.W., Hessels, J.W.T., Hoeft, M., Hörandel, J., Iacobelli, M., Juette, E., Kondratiev, V.I., Kuniyoshi, M., Kuper, G., Leeuwen, J., Loose, M., Maat, P., Mann, G., Markoff, S., Mcfadden, R., Mckay-Bukowski, D., Moldon, J., Munk, H., Nelles, A., Norden, M.J., Orru, E., Paas, H., Pandey-Pommier, M., Pizzo, R., Polatidis, A.G., Reich, W., Röttgering, H., Rowlinson, A., Schwarz, D., Smirnov, O., Steinmetz, M., Swinbank, J., Tagger, M., Thoudam, S., Toribio, M.C., Vermeulen, R., Vocks, C., Weeren, R.J., Wijers, R.A.M.J., Wucknitz, O.: Imaging Jupiter's radiation belts down to 127 MHz with LOFAR. Astron. Astrophys. - A&A. **587**, 3 (2016). https://doi.org/10.1051/0004-6361/201527518
20. Bhardwaj, A., Ishwara-Chandra, C.H., Udaya Shankar, N., Misawa, H., Imai, K., Miyoshi, Y., Tsuchiya, F., Kondo, T., Morioka, A.: GMRT observations of jupiter's synchrotron radio emission at 610 MHz. In: Saikia, D.J., Green, D.A., Gupta, Y., Venturi, T. (eds.) The low-frequency radio universe. Astronomical society of the pacific conference series, vol. 407, p. 369 (2009)
21. Khurana, K., Vasyliūnas, V., Mauk, B., Frank, L., Paterson, B., Kivelson, M., Krupp, N., Woch, J., Lagg, A., Kurth, B.: The configuration of jupiter's magnetosphere. Jupiter: the planet, satellites and magnetosphere, 593-616 (2004). (2004)
22. Vogt, R.E., Cook, W.R., Cummings, A.C., Garrard, T.L., Gehrels, N., Stone, E.C., Trainor, J.H., Schardt, A.W., Conlon, T., Lal, N., McDonald, F.B.: Voyager 1: Energetic ions and electrons in the jovian magnetosphere. Sci. **204**(4396), 1003–1007 (1979). https://doi.org/10.1126/science.204.4396.1003
23. Bolton, S.J.: The juno mission. Proc. Int. Astron. Congr. Union. **6**(S269), 92–100 (2010). https://doi.org/10.1017/S1743921310007313
24. Roussos, E., Kollmann, P., Krupp, N., Kotova, A., Regoli, L., Paranicas, C., Mitchell, D.G., Krimigis, S.M., Hamilton, D., Brandt, P., Carbary, J., Christon, S., Dialynas, K., Dandouras, I., Hill, M.E., Ip, W.H., Jones, G.H., Livi, S., Mauk, B.H., Palmaerts, B., Roelof, E.C., Rymer, A., Sergis, N., Smith, H.T.: A radiation belt of energetic protons located between saturn and its rings. Sci. **362**(6410), 1962 (2018). https://doi.org/10.1126/science.aat1962
25. Kollmann, P., Roussos, E., Kotova, A., Regoli, L., Mitchell, D.G., Carbary, J., Clark, G., Krupp, N., Paranicas, C.: Saturn's innermost radiation belt throughout and inward of the D-Ring. Geophys. Res. Lett. **45**, 10912–10920 (2018). https://doi.org/10.1029/2018GL077954
26. Comprehensive Observations of Magnetospheric Particle Acceleration, Sources, and Sinks (COMPASS): a mission concept to jupiter's extreme magnetosphere to address fundamental mysteries in heliophysics. http://surveygizmoresponseuploads.s3.amazonaws.com/fileuploads/623127/6920789/202-1ec7e3cd1d519ac59b45e11010a8a8e2_ClarkGeorgeB.pdf. White Paper for the 2024-2033 Solar and Space Physics (Heliophysics) Decadal Survey, Accessed 27 Oct 2022
27. Turner, D., Clark, G., Li, W., Blum, L., Kollmann, P., Jaynes, A., Marshall, R., Ukhorskiy, A., Berland, G., Cohen, I., Drozdov, A., Dunn, W., Hospodarsky, G., Kraft, R., Li, X., Looper, M., Mauk, B., Nenon, Q., O'Brien, P., Roussos, E., Smith, H.T., Sorathia, K., Williams, P., Wu, X.: Comprehensive observations of magnetospheric particle acceleration, sources and sinks (compass) pre-study report. (2021)
28. Hao, Y.-X., Sun, Y.-X., Roussos, E., Liu, Y., Kollmann, P., Yuan, C.-J., Krupp, N., Paranicas, C., Zhou, X.-Z., Murakami, G., Kita, H., Zong, Q.-G.: The formation of saturn's and jupiter's electron radiation belts by magnetospheric electric fields. Astrophys. J. Lett. **905**(1), 10 (2020). https://doi.org/10.3847/2041-8213/abca3f
29. Baker, D., Kanekal, S., Hoxie, V., Batiste, S., Bolton, M., Li, X., Elkington, S., Monk, S., Reukauf, R., Steg, S., Westfall, J., Belting, C., Bolton, B., Braun, D., Cervelli, B., Hubbell, K., Kien, M., Knappmiller, S., Wade, S., Friedel, R.: The relativistic electron-proton telescope (rept) instrument on

board the radiation belt storm probes (rbsp) spacecraft: characterization of earth's radiation belt high-energy particle populations. Space Sci. Rev. **179** (2012). https://doi.org/10.1007/s11214-012-9950-9

30. Mazur, J., Friesen, L., Lin, A., Mabry, D., Katz, N., Dotan, Y., George, J., Blake, J., Looper, M., Redding, M., O'Brien, T., Cha, J., Birkitt, A., Carranza, P., Lalic, M., Fuentes, F., Galvan, R., McNab, M.: The relativistic proton spectrometer (rps) for the radiation belt storm probes mission. Space Sci. Rev. **179** (2012). https://doi.org/10.1007/s11214-012-9926-9
31. Nenon, Q., Sicard, A., Bourdarie, S.: A new physical model of the electron radiation belts of jupiter inside europa's orbit. J. Geophys. Res. Space Phys. **122**(5), 5148–5167 (2017). https://doi.org/10.1002/2017JA023893
32. Nenon, Q., Sicard, A., Kollmann, P., Garrett, H.B., Sauer, S.P.A., Paranicas, C.: A physical model of the proton radiation belts of jupiter inside europa's orbit. J. Geophys. Res. Space Phys. **123**(5), 3512–3532 (2018). https://doi.org/10.1029/2018JA025216
33. Wu, X., Ambrosi, G., Azzarello, P., Bergmann, B., Bertucci, B., Cadoux, F., Campbell, M., Duranti, M., Ionica, M., Kole, M., Krucker, S., Maehlum, G., Meier, D., Paniccia, M., Pinsky, L., Plainaki, C., Pospisil, S., Stein, T., Thonet, P.A., Tomassetti, N., Tykhonov, A.: Penetrating particle analyzer (pan). Adv. Space Res. **63**(8), 2672–2682 (2019). https://doi.org/10.1016/j.asr.2019.01.012
34. Stone, E.C., Cohen, C.M.S., Cook, W.R., Cummings, A.C., Gauld, B., Kecman, B., Leske, R.A., Mewaldt, R.A., Thayer, M.R., Dougherty, B.L., Grumm, R.L., Milliken, B.D., Radocinski, R.G., Wiedenbeck, M.E., Christian, E.R., Shuman, S.A., Trexel, H., Rosenvinge, T.T., Binns, W.R., Crary, D.J., Dowkontt, P.F., Epstein, J.E., Hink, P.L., Klarmann, J., Lijowski, M., Olevitch, M.A.: The cosmic-ray isotope spectrometer for the advanced composition explorer. Space Sci. Rev. **86**, 285–356 (1998)
35. Stone, E.C., Cummings, A.C., McDonald, F.B., Heikkila, B.C., Lal, N., Webber, W.R.: Voyager 1 observes low-energy galactic cosmic rays in a region depleted of heliospheric ions. Sci. **341**(6142), 150–153 (2013). https://doi.org/10.1126/science.1236408
36. Spence, H., Case, A., Golightly, M., Heine, T., Larsen, B., Blake, J., Caranza, P., Crain, W., George, J., Lalic, M., Lin, A., Looper, M., Mazur, J., Salvaggio, D., Kasper, J., Stubbs, T., Doucette, M., Ford, P., Foster, R., Charara, Y.: Crater: The cosmic ray telescope for the effects of radiation experiment on the lunar reconnaissance orbiter mission. Space Sci. Rev. **150**, 243–284 (2010). https://doi.org/10.1007/s11214-009-9584-8
37. Kunow, H., Fischer, H., Green, G., Mueller-Mellin, R., Wibberenz, G., Holweger, H., Evenson, P., Meyer, J.-P., Hasebe, N., von Rosenvinge, T.: COSTEP: a comprehensive suprathermal and energetic particle analyzer for SOHO. In ESA, The SOHO Mission. Scientific and Technical Aspects of the Instruments p 75-80 (SEE N90-13302 04-92) (1988)
38. Geostationary Satellites. https://www.nesdis.noaa.gov/current-satellite-missions/currently-flying/geostationary-satellites. Accessed 26 Sep 2022
39. Pinto, M., Goncalves, P., Hajdas, W., Socha, P.: The RADiation hard Electron Monitor (RADEM) for the JUICE mission. In: European Planetary Science Congress, pp. 2020–311 (2020). https://doi.org/10.5194/epsc2020-311
40. Picozza, P., Galper, A.M., Castellini, G., Adriani, O., Altamura, F., Ambriola, M., Barbarino, G.C., Basili, A., Bazilevskaja, G.A., Bencardino, R., Boezio, M., Bogomolov, E.A., Bonechi, L., Bongi, M., Bongiorno, L., Bonvicini, V., Cafagna, F., Campana, D., Carlson, P., Casolino, M., De Marzo, C., De Pascale, M.P., De Rosa, G., Fedele, D., Hofverberg, P., Koldashov, S.V., Krutkov, S.Y., Kvashnin, A.N., Lund, J., Lundquist, J., Maksumov, O., Malvezzi, V., Marcelli, L., Menn, W., Mikhailov, V.V., Minori, M., Misin, S., Mocchiutti, E., Morselli, A., Nikonov, N.N., Orsi, S., Osteria, G., Papini, P., Pearce, M., Ricci, M., Ricciarini, S.B., Runtso, M.F., Russo, S., Simon, M., Sparvoli, R., Spillantini, P., Stozhkov, Y.I., Taddei, E., Vacchi, A., Vannuccini, E., Voronov, S.A., Yurkin, Y.T., Zampa, G., Zampa, N., Zverev, V.G.: Pamela - a payload for antimatter matter exploration and light-nuclei astrophysics. Astropart. Phys. **27**(4), 296–315 (2007). https://doi.org/10.1016/j.astropartphys.2006.12.002
41. Lübelsmeyer, K., Schultz von Dratzig, A., Wlochal, M., Ambrosi, G., Azzarello, P., Battiston, R., Becker, R., Becker, U., Bertucci, B., Bollweg, K., Burger, J.D., Cadoux, F., Cai, X.D., Capell, M., Choutko, V., Duranti, M., Gargiulo, C., Guandalini, C., Haino, S., Ionica, M., Koulemzine, A., Kounine, A., Koutsenko, V., Laurenti, G., Lebedev, A., Martin, T., Oliva, A., Paniccia, M., Perrin, E., Rapin, D., Rozhkov, A., Schael, S., Tholen, H., Ting, S.C.C., Zuccon, P.: Upgrade of the alpha magnetic spectrometer (ams-02) for long term operation on the international space station (iss). Nuclear Instruments and Methods in Physics Research Section A: Accelerators, Spectrometers, Detectors and Associated Equipment. **654**(1), 639–648 (2011). https://doi.org/10.1016/j.nima.2011.06.051

42. Development of a demonstrator for the Penetrating Particle Analyser (PAN) technology. https://cordis.europa.eu/project/id/862044. Accessed 25 Sep 2022
43. Silari, M., Campbell, M., Rosenfeld, A.: The Medipix/Timepix ASIC Family and Its Applications. Elsevier, ??? (2020). This Special Issue is dedicated to Medipix and Timepix semiconductor radiation detectors whose origins lie in the R & D for the semiconductor tracking detectors of the Large Hadron Collider at CERN. https://cds.cern.ch/record/2744734
44. Llopart, X., Alozy, J., Ballabriga, R., Campbell, M., Casanova, R., Gromov, V., Heijne, E.H.M., Poikela, T., Santin, E., Sriskaran, V., Tlustos, L., Vitkovskiy, A.: Timepix4, a large area pixel detector readout chip which can be tiled on 4 sides providing sub-200 ps timestamp binning. J. Instrum. **17**(01), 01044 (2022). https://doi.org/10.1088/1748-0221/17/01/c01044
45. Samin, A.J.: A review of radiation-induced demagnetization of permanent magnets. Journal of Nuclear Materials. **503**, 42–55 (2018). https://doi.org/10.1016/j.jnucmat.2018.02.029
46. Shepherd, B.: Radiation damage to permanent magnet materials: A survey of experimental results. Technical report, CERN, Geneva (2018). https://cds.cern.ch/record/2642418
47. Okuda, S., Ohashi, K., Kobayashi, N.: Effects of electron-beam and γ-ray irradiation on the magnetic flux of ndfeb and smco permanent magnets. Nuclear instruments and methods in physics research section B: Beam interactions with materials and atoms. **94**(3), 227–230 (1994). https://doi.org/10.1016/0168-583X(94)95358-9
48. Bizen, T., Marechal, X., Seike, T., Asano, Y., Dong, E.K., Lee, H.-S., Hara, T., Kitamura, H., Tanaka, T.: Radiation Damage in Magnets for Undulators at Low Temperature, 3 (2004)
49. Medipix Collaboration. https://medipix.web.cern.ch/. Accessed 20 Mar 2023
50. Poikela, T., Plosila, J., Westerlund, T., Campbell, M., Gaspari, M.D., Llopart, X., Gromov, V., Kluit, R., Beuzekom, M., Zappon, F., Zivkovic, V., Brezina, C., Desch, K., Fu, Y., Kruth, A.: Timepix3: a 65k channel hybrid pixel readout chip with simultaneous ToA/ToT and sparse readout. J. Instrum. **9**(05), 05013–05013 (2014). https://doi.org/10.1088/1748-0221/9/05/c05013
51. Burian, P., Broulim, P., Bergmann, B.: Study of power consumption of timepix3 detector. J. Instrum. **14**(01), 01001–01001 (2019). https://doi.org/10.1088/1748-0221/14/01/c01001
52. Pinsky, L.S., Pospisil, S.: Timepix-based detectors in mixed-field charged-particle radiation dosimetry applications. Radiat. Meas. **138**, 106229 (2020). https://doi.org/10.1016/j.radmeas.2019.106229
53. Stoffle, N.N., Campbell-Ricketts, T., Castro, A., Gaza, R., Zeitlin, C., George, S., Abdelmelek, M., Schram, A.: Hera: A timepix-based radiation detection system for exploration-class space missions. Life Sci. Space Res. (2023). https://doi.org/10.1016/j.lssr.2023.03.004
54. Gluckstern, R.L.: Uncertainties in track momentum and direction, due to multiple scattering and measurement errors. Nucl. Inst. Methods. **24**, 381–389 (1963). https://doi.org/10.1016/0029-554X(63)90347-1
55. Agostinelli, S., Allison, J., Amako, K., Apostolakis, J., Araujo, H., Arce, P., Asai, M., Axen, D., Banerjee, S., Barrand, G., Behner, F., Bellagamba, L., Boudreau, J., Broglia, L., Brunengo, A., Burkhardt, H., Chauvie, S., Chuma, J., Chytracek, R., Cooperman, G., Cosmo, G., Degtyarenko, P., Dell'Acqua, A., Depaola, G., Dietrich, D., Enami, R., Feliciello, A., Ferguson, C., Fesefeldt, H., Folger, G., Foppiano, F., Forti, A., Garelli, S., Giani, S., Giannitrapani, R., Gibin, D., Gómez Cadenas, J.J., Gonzalez, I., Gracia Abril, G., Greeniaus, G., Greiner, W., Grichine, V., Grossheim, A., Guatelli, S., Gumplinger, P., Hamatsu, R., Hashimoto, K., Hasui, H., Heikkinen, A., Howard, A., Ivanchenko, V., Johnson, A., Jones, F.W., Kallenbach, J., Kanaya, N., Kawabata, M., Kawabata, Y., Kawaguti, M., Kelner, S., Kent, P., Kimura, A., Kodama, T., Kokoulin, R., Kossov, M., Kurashige, H., Lamanna, E., Lampen, T., Lara, V., Lefebure, V., Lei, F., Liendl, M., Lockman, W., Longo, F., Magni, S., Maire, M., Medernach, E., Minamimoto, K., Mora de Freitas, P., Morita, Y., Murakami, K., Nagamatu, M., Nartallo, R., Nieminen, P., Nishimura, T., Ohtsubo, K., Okamura, M., O'Neale, S., Oohata, Y., Paech, K., Perl, J., Pfeiffer, A., Pia, M.G., Ranjard, F., Rybin, A., Sadilov, S., Di Salvo, E., Santin, G., Sasaki, T., Savvas, N., Sawada, Y., Scherer, S., Sei, S., Sirotenko, V., Smith, D., Starkov, N., Stoecker, H., Sulkimo, J., Takahata, M., Tanaka, S., Tcherniaev, E., Safai Tehrani, E., Tropeano, M., Truscott, P., Uno, H., Urban, L., Urban, P., Verderi, M., Walkden, A., Wander, W., Weber, H., Wellisch, J.P., Wenaus, T., Williams, D.C., Wright, D., Yamada, T., Yoshida, H., Zschiesche, D.: Geant4-a simulation toolkit. Nuclear Instruments and Methods in Physics Research Section A: Accelerators, Spectrometers, Detectors and Associated Equipment. **506**(3), 250–303 (2003). https://doi.org/10.1016/S0168-9002(03)01368-8
56. GenFit Package. https://github.com/GenFit/GenFit. Accessed 19 Sep 2022
57. Adriani, O., Barbarino, G.C., Bazilevskaya, G.A., Bellotti, R., Boezio, M., Bogomolov, E.A., Bongi, M., Bonvicini, V., Borisov, S., Bottai, S., Bruno, A., Cafagna, F., Campana, D., Carbone, R., Carlson, P.,

Casolino, M., Castellini, G., Consiglio, L., Pascale, M.P.D., Santis, C.D., Simone, N.D., Felice, V.D., Galper, A.M., Gillard, W., Grishantseva, L., Jerse, G., Karelin, A.V., Kheymits, M.D., Koldashov, S.V., Krutkov, S.Y., Kvashnin, A.N., Leonov, A., Malakhov, V., Marcelli, L., Mayorov, A.G., Menn, W., Mikhailov, V.V., Mocchiutti, E., Monaco, A., Mori, N., Nikonov, N., Osteria, G., Palma, F., Papini, P., Pearce, M., Picozza, P., Pizzolotto, C., Ricci, M., Ricciarini, S.B., Rossetto, L., Sarkar, R., Simon, M., Sparvoli, R., Spillantini, P., Stozhkov, Y.I., Vacchi, A., Vannuccini, E., Vasilyev, G., Voronov, S.A., Yurkin, Y.T., Wu, J., Zampa, G., Zampa, N., Zverev, V.G.: The discovery of geomagnetically trapped cosmic-ray antiprotons. Astrophys. J. **737**(2), 29 (2011). https://doi.org/10.1088/2041-8205/737/2/l29

58. Blake, J.B., Schulz, M.: The satellites of jupiter as a source of very energetic magnetospheric particles. Icarus. **44**(2), 367–372 (1980). https://doi.org/10.1016/0019-1035(80)90031-7
59. Clark, G., Mauk, B.H., Kollmann, P., Paranicas, C., Bagenal, F., Allen, R.C., Bingham, S., Bolton, S., Cohen, I., Ebert, R.W., Dunn, W., Haggerty, D., Houston, S.J., Jackman, C.M., Roussos, E., Rymer, A., Westlake, J.H.: Heavy ion charge states in jupiter's polar magnetosphere inferred from auroral megavolt electric potentials. J. Geophys. Res. Space Phys. **125**(9), 2020–028052 (2020). https://doi.org/10.1029/2020JA028052.e2020JA0280522020JA028052
60. Mauk, B.H., Mitchell, D.G., McEntire, R.W., Paranicas, C.P., Roelof, E.C., Williams, D.J., Krimigis, S.M., Lagg, A.: Energetic ion characteristics and neutral gas interactions in jupiter's magnetosphere. J. Geophys. Res. Space Phys. **109**(A9) (2004). https://doi.org/10.1029/2003JA010270
61. Nenon, Q., Sicard, A., Caron, P.: The rings of jupiter as seen by the electron and proton radiation belt model salammbô. Geophys. Res. Lett. **45**(20), 10838–10846 (2018). https://doi.org/10.1029/2018GL080157
62. Pinsky, L.S., Empl, A., Gutierrez, A., Jakubek, J., Kitamura, H., Miller, J., Leroy, C., Stoffle, N., Pospisil, S., Uchihori, Y., Yasuda, N., Zeitlin, C.: Penetrating heavy ion charge and velocity discrimination with a timepix-based si detector (for space radiation applications). Nuclear Instruments and Methods in Physics Research Section A: Accelerators, Spectrometers, Detectors and Associated Equipment. **633**, 190–193 (2011). 11th International Workshop on Radiation Imaging Detectors (IWORID) https://doi.org/10.1016/j.nima.2010.06.164
63. Schön, R., Alfonsi, M., van Bakel, N., van Beuzekom, M., Koffeman, E.: Cool timepix – electronic noise of the timepix readout chip down to -125°c. Nuclear instruments and methods in physics research Section A: Accelerators, spectrometers, detectors and associated equipment. **771**, 74–77 (2015). https://doi.org/10.1016/j.nima.2014.10.063
64. Urban, M., Doubravova, D.: Timepix3: temperature influence on x-ray measurements in counting mode with si sensor. Radiat Meas. **141**, 106535 (2021). https://doi.org/10.1016/j.radmeas.2021.106535
65. Sicard-Piet, A., Bourdarie, S., Krupp, N.: Jose: A new jovian specification environment model. IEEE Trans. Nucl Sci. **58**(3), 923–931 (2011). https://doi.org/10.1109/TNS.2010.2097276
66. Ashmanskas, W., Bardi, A., Bari, M., Belforte, S., Berryhill, J., Bogdan, M., Cerri, A., Clark, A.G., Chlanchidze, G., Condorelli, R., Culbertson, R., Dell'Orso, M., Donati, S., Frisch, H.J., Galeotti, S., Giannetti, P., Glagolev, V., Leger, A., Meschi, E., Morsani, F., Nakaya, T., Punzi, G., Ristori, L., Sanders, H., Semenov, A., Signorelli, G., Shochet, M., Speer, T., Spinella, F., Wilson, P., Wu, X., Zanetti, A.M.: Silicon vertex tracker: A fast precise tracking trigger for cdf. Nuclear instruments and methods in physics research section A: Accelerators, spectrometers, detectors and associated equipment. **447**(1), 218–222 (2000). https://doi.org/10.1016/S0168-9002(00)00190-X
67. Aad, G., et al.: The ATLAS Fast TracKer system. JINST. **16**, 07006 (2021). https://doi.org/10.1088/1748-0221/16/07/P07006. arXiv:2101.05078 [physics.ins-det]

Authors and Affiliations

Johannes Hulsman[1] · Xin Wu[1] · Philipp Azzarello[1] · Benedikt Bergmann[2] · Michael Campbell[3] · George Clark[4] · Franck Cadoux[1] · Tomoya Ilzawa[1] · Peter Kollmann[4] · Xavi Llopart[3] · Quentin Nénon[5] · Mercedes Paniccia[1] · Elias Roussos[6] · Petr Smolyanskiy[2] · Daniil Sukhonos[1] · Pierre Alexandre Thonet[7]

Philipp Azzarello
philipp.azzarello@unige.ch

Benedikt Bergmann
benedikt.bergmann@utef.cvut.cz

Michael Campbell
michael.campbell@cern.ch

George Clark
George.Clark@jhuapl.edu

Franck Cadoux
franck.cadoux@unige.ch

Tomoya Ilzawa
tomoya.ilzawa@unige.ch

Peter Kollmann
Peter.Kollmann@jhuapl.edu

Xavi Llopart
Xavier.Llopart@cern.ch

Quentin Nénon
q.nenon@gmail.com

Mercedes Paniccia
Mercedes.Paniccia@cern.ch

Elias Roussos
roussos@mps.mpg.de

Petr Smolyanskiy
petr.smolyanskiy@cvut.cz

Daniil Sukhonos
daniil.sukhonos@unige.ch

Pierre Alexandre Thonet
pierre.alexandre.thonet@cern.ch

1 DPNC, University of Geneva, 24 Quai Ernest-Ansermet, CH-1205 Geneva, Switzerland

2 Institute of Experimental and Applied Physics, Czech Technical University in Prague, Husova 240/5, 110 00 Prague, Czech Republic

3 EP Department, CERN, 23, CH-1211 Geneva, Switzerland

4 Johns Hopkins University Applied Physics Laboratory, Laurel MD 20723-6099, USA

5 Institut de Recherche en Astrophysique et Planétologie, CNRS-UPS-CNES, 31400 Toulouse, France

6 Max Planck Institute for Solar System Research, Justus-von-Liebig-Weg 3, 37077 Göttingen, Germany

7 TE Department, CERN, 23, CH-1211 Geneva, Switzerland